Extension of scattering theory for finite times: Three-body scattering

T. Petrosky,[1,2] G. Ordonez,[1] and T. Miyasaka[3]
[1]*Center for Studies in Statistical Mechanics and Complex Systems, The University of Texas at Austin, Austin, Texas 78712*
[2]*International Solvay Institutes, Code Postal 231, 1050 Brussels, Belgium*
[3]*Department of Applied Physics, Waseda University, Tokyo, Japan*
(Received 20 September 1995)

Scattering theory is extended to the description of processes during collision. Indeed, for large wave packets we may consider situations where time t, while large with respect to characteristic frequencies, is still smaller than the duration of the collision t_c. This leads to an asymptotic theory which is different from the usual S-matrix approach. There appear intermediate states with scattering cross sections which result from secular effects for $t<t_c$, but differ from the values obtained for $t>t_c$ in the S-matrix theory. The consideration of such intermediate time scales is the normal procedure in many-body situations as realized, for example, in chemical reactions. Our method is closely connected to our work on the extension of quantum theory beyond the Hilbert space for large Poincaré systems. This theory applies to persistent scattering using delocalized density matrices (an example is plane waves). For this case, the S-matrix theory is not valid, while the results of our asymptotic approach remain valid for all times. Our theoretical predictions have been validated by numerical simulations. [S1050-2947(96)06405-0]

PACS number(s): 03.80.+r, 03.65.Bz, 05.30.−d, 11.80.Jy

I. INTRODUCTION

In the standard theory of scattering (see, e.g., [1–4]) one considers asymptotically free in and out states interacting during a finite time t_c. This leads to an S-matrix description of the collision process which is valid for times of observation t larger than t_c. For large wave packets, we may consider different situations where t, while large with respect to characteristic frequencies, is smaller than t_c. This leads to an asymptotic theory which is different from the usual S-matrix approach. There may now appear ''intermediate'' states which result from *secular effects* for $t \ll t_c$ but vanish for $t \gg t_c$. The consideration of such intermediate time scales is the normal procedure in many-body situations, as realized, for example, in chemical reactions.

We shall concentrate in this paper on three-body scattering. However, we first briefly consider two-body scattering as it permits us to introduce the main concepts leading to our asymptotic approach (Sec. III). We calculate the transition probability starting from large wave packets. As is well known, the scattered wave packet has a sharp peak at resonance, and a small tail effect coming from the off-resonance-shell contribution. The value of the off-shell contribution differs in the two asymptotic situations corresponding to $t \gg t_c$ (S matrix) and $t \ll t_c$ (obtained by our approach).

For a typical momentum k (with $\hbar=1$ and mass $m=1$), the duration of the collision is given by $t_c \sim (|k|\eta)^{-1}$, where $1/\eta$ is the size of the wave packet in configuration space. Then one can summarize the two different asymptotic limits used in our paper in Table I, where $\epsilon \sim 1/t$. It is very interesting that the extension of scattering theory to finite times, corresponding to the statistical-mechanics approach, can only be performed on the level of density matrices and *not* on the level of wave functions. The reason is that the transition probability can no more be factorized into a product of wave functions. We shall come back to this important point below (Sec. IX).

We then come to three-body scattering (Secs. IV–VIII). For simplicity, we consider scattering in one dimension, and assume repulsive δ-function interactions. Extensions to more general situations are easy. In this case even the *secular* terms are different in the two asymptotic situations.

We work in center-of-mass system, and use Jacobi's coordinates and momenta (see [5,6]). We can then transform the problem into the study of the evolution of a single particle in *two-dimensional* space interacting with three walls. We obtain a simple pictorial description of the scattering processes (see Sec. IV). We concentrate our attention on the process corresponding to an interaction between particles 1 and 2 followed by an interaction between 2 and 3. We study this process in Liouville space, which permits a clear separation of rescattering effects from genuine three-body effects. In fact, this is the lowest order interaction, which involves both successive two-body scattering, as well as genuine irreducible three-body effects [6–8].

We calculate the various contributions leading to secular effects starting again from large wave packets. Now our asymptotic theory leads to a dramatic effect as classes of secular effects appear only for $t \ll t_c$, and disappear in the frame of the S-matrix theory for $t \gg t_c$. Our results have been confirmed by numerical simulations.

As a result of this effect, the scattering three-body cross section is different in the two situations. This result is closely connected to our work on the extension of quantum theory beyond the Hilbert space for large Poincaré systems (LPS's) [9,10]. This theory applies to persistent scattering using de-

TABLE I. Two different asymptotic limits: S-matrix approach and statistical-mechanics approach.

S-matrix approach	Stat. mech. approach
$\|k\|\eta \gg \epsilon$	$\|k\|\eta \ll \epsilon$
first $t\to\infty$ then $\eta\to 0$	first $\eta\to 0$ then $t\to\infty$

localized density matrices (for example, plane waves). In the frame of our asymptotic theory for $t \ll t_c$, the system still does not ''know'' if we started with a large but finite wave packet, or if we started with a delocalized density matrix. Persistent interactions require singular distribution functions (i.e., the δ-function singularity in momentum), which lie outside the Hilbert space. The S-matrix theory is no longer valid. We have then obtained complex, irreducible spectral representations of the evolution operators, here the Liouville operator L_H, in generalized function spaces [9,10]. The results of our asymptotic approach then remain valid for all times. Our theory also removes the rescattering anomaly, which is due to successive two-body collision in three-body scattering. As this problem has a long history, we shall present it in a separate paper [11], and only mention it briefly in this paper.

In the two asymptotic theories, the results obtained for the three-body scattering cross sections are different. As mentioned, in this paper we concentrate on a single process [a (12) interaction followed by a (23) interaction]. It is easy to extend our results to other three-body processes. In a subsequent paper, we shall consider all three-body scattering processes, and give an explicit expression for the difference in the cross sections.

II. LIOUVILLE SPACE FORMALISM

We consider nonrelativistic quantum systems of N distinguishable particles with $N=2$ and 3 in d-dimensional space. Before going to a specific number N, we first introduce notations for arbitrary finite N. For $N \to \infty$, see [10]. In the center-of-mass (CM) frame, the number of degrees of freedom reduces to $M \equiv (N-1)d$. In the CM frame the Hamiltonian is given by (we shall use a unit system with $\hbar=1$)

$$H = H_0 + \lambda V, \tag{2.1}$$

where H_0 is the unperturbed Hamiltonian associated with free motion, and λ is a dimensionless positive coupling constant. In this paper we consider a short-range repulsive interaction λV among the particles. There are no bound states. In the CM frame we shall use vector notation, such as $\mathbf{x}=(x_1,\ldots,x_M)$.

We denote the eigenstates of H_0 by $|\mathbf{k}\rangle$, i.e.,

$$H_0|\mathbf{k}\rangle = \omega_k|\mathbf{k}\rangle. \tag{2.2}$$

They satisfy

$$\int d^M k |\mathbf{k}\rangle\langle\mathbf{k}| = 1, \quad \langle\mathbf{p}|\mathbf{k}\rangle = \delta(\mathbf{p}-\mathbf{k}) = \prod_{i=1}^{M} \delta(p_i - k_i), \tag{2.3}$$

where $d^M k \equiv dk_1 \ldots dk_M$, and $\delta(p_i - k_i)$ is the Dirac δ function. We assume

$$\omega_k \equiv \sum_{i=1}^{M} \omega_{k_i}. \tag{2.4}$$

For example, we have a Hamiltonian (3.1) for potential scattering that corresponds to two-body scattering, and a Hamiltonian (4.9) represented by Jacobi's coordinates that corresponds to three-body scattering.

The evolution of the system is governed by the Liouville–von Neumann equation for the density matrix ρ [12],

$$i \frac{\partial}{\partial t} \rho(t) = L_H \rho(t), \tag{2.5}$$

where L_H is the Liouville–von Neumann operator (the Liouvillian in short) that is the commutator with the Hamiltonian $L_H \rho = [H, \rho]$.

The formal solution of the Liouville–von Neumann equation is

$$\rho(t) = \mathscr{U}(t)\rho(0), \tag{2.6}$$

with

$$\mathscr{U}(t) = e^{-iL_H t}. \tag{2.7}$$

$\mathscr{U}(t)$ is the evolution operator and obeys the integral equation

$$\mathscr{U}(t) = e^{-iL_0 t} - i\lambda \int_0^t dt' e^{-iL_0(t-t')} L_V \mathscr{U}(t'), \tag{2.8}$$

where L_0 is the unperturbed Liouvillian $L_0 \equiv L_{H_0}$, and L_V is the interaction Liouvillian,

$$L_H = L_0 + \lambda L_V. \tag{2.9}$$

We can write the formal solution of (2.8) for $t>0$ in terms of the Laplace transformation as [12]

$$\mathscr{U}(t) = \frac{1}{2\pi i} \int_C dz\ e^{-izt} R(z), \tag{2.10}$$

where $R(z)$ is the resolvent operator for the Liouvillian defined by

$$R(z) \equiv \frac{1}{z - L_H}, \tag{2.11}$$

and C is a contour which runs from $+\infty$ to $-\infty$, parallel to and above the real axis. This satisfies the resolvent equation

$$R(z) = R_0(z) + R_0(z)\lambda L_V R(z), \tag{2.12}$$

where $R_0(z)$ is the unperturbed resolvent operator defined by

$$R_0(z) \equiv \frac{1}{z - L_0}. \tag{2.13}$$

We may introduce the $\mathscr{T}$ matrix for the Liouvillian in the Liouville space in analogy to the usual scattering theory formulated for the Hamiltonian. This satisfies the integral equation

$$\mathscr{T}(z) = \lambda L_V + \lambda L_V R_0(z) \mathscr{T}(z). \tag{2.14}$$

Assuming the convergence, the iterative solution of (2.14) is given by

$$\mathscr{T}(z)=\sum_{n=0}^{\infty}\lambda L_V[R_0(z)\lambda L_V]^n. \tag{2.15}$$

This then leads to

$$\mathscr{U}(t)=\frac{1}{2\pi i}\int_C dz\ e^{-izt}\sum_{n=0}^{\infty}[R_0(z)\lambda L_V]^n R_0(z). \tag{2.16}$$

For scattering of a wave packet, which the usual S-matrix theory deals with, the interaction is transient. As the wave function Ψ is localized in configuration space, it has a well-defined norm,

$$||\Psi||=\left(\int d^M x|\langle\mathbf{x}|\Psi\rangle|^2\right)^{1/2}<\infty. \tag{2.17}$$

In this situation, the Liouville–von Neumann equation does not introduce any new features. If we can integrate Schrödinger's equation, we can solve the Liouville–von Neumann equation, and vice versa. Usually, one equips the Liouville space with a Hilbert space structure. In this space a scalar product of the linear operators A and B acting on wave functions is defined as a Schmidt inner product

$$\langle\langle A|B\rangle\rangle\equiv\mathrm{Tr}(A^\dagger B), \tag{2.18}$$

and its Hilbert norms by

$$||A||\equiv\sqrt{\langle\langle A|A\rangle\rangle}. \tag{2.19}$$

We have also introduced Dirac's ''bra'' and ''ket'' notations, i.e., $\langle\langle A|$ and $|B\rangle\rangle$, analogous to the notations used for wave functions. For example, the Hilbert norm for the density matrix associated with the wave packet $\rho=\Psi\Psi^*$ is given by

$$||\rho||=\int d^M x|\langle\mathbf{x}|\Psi\rangle|^2<\infty. \tag{2.20}$$

The Liouvillian L_H is then a Hermitian operator, and $\mathscr{U}(t)$ is unitary.

In the Liouville space we denote dyadic operators $|\mathbf{p}\rangle\langle\mathbf{p}'|$ generated by the eigenstates $|\mathbf{p}\rangle$ and $|\mathbf{p}'\rangle$ of H_0 by a ket state,

$$|\mathbf{p};\mathbf{p}'\rangle\rangle\equiv|\mathbf{p}\rangle\langle\mathbf{p}'|. \tag{2.21}$$

They form a complete orthonormal set of the Liouville space,

$$\int d\mathbf{p}\int d\mathbf{p}'|\mathbf{p};\mathbf{p}'\rangle\rangle\langle\langle\mathbf{p};\mathbf{p}'|=\int d\mathbf{p}\int d\mathbf{p}'|\mathbf{p}\rangle\langle\mathbf{p}|\times|\mathbf{p}'\rangle\langle\mathbf{p}'|=1,$$

$$\langle\langle\mathbf{p};\mathbf{p}'|\mathbf{k};\mathbf{k}'\rangle\rangle=\delta(\mathbf{p}-\mathbf{k})\,\delta(\mathbf{k}'-\mathbf{p}'). \tag{2.22}$$

They are eigenstates of L_0,

$$L_0|\mathbf{p};\mathbf{p}'\rangle\rangle=H_0|\mathbf{p}\rangle\langle\mathbf{p}'|-|\mathbf{p}\rangle\langle\mathbf{p}'|H_0=w_{pp'}|\mathbf{p};\mathbf{p}'\rangle\rangle, \tag{2.23}$$

where

$$w_{pp'}\equiv\omega_p-\omega_{p'}. \tag{2.24}$$

In this representation we have a simple expression for matrix elements of operator A acting on wave functions [see (2.18)]:

$$A_{\mathbf{pp}'}=\langle\mathbf{p}|A|\mathbf{p}'\rangle=\langle\langle\mathbf{p};\mathbf{p}'|A\rangle\rangle. \tag{2.25}$$

The operators acting on density matrices are called super operators. A factorizable super operator $A\times B$ is defined by

$$(A\times B)\rho=A\rho B, \tag{2.26}$$

where A and B are linear operators in wave-function space. The Liouvillian is then

$$L_H=H\times 1-1\times H. \tag{2.27}$$

The matrix element of the perturbed Liouvillian is given by

$$\langle\langle\mathbf{p};\mathbf{p}'|L_V|\mathbf{p}'';\mathbf{p}'''\rangle\rangle=V_{\mathbf{pp}''}\delta(\mathbf{p}'''-\mathbf{p}')-\delta(\mathbf{p}-\mathbf{p}'')V_{\mathbf{p}'''\mathbf{p}'}. \tag{2.28}$$

In this paper we shall consider the scattering problem for two classes of density matrices; in one class the Hilbert norms converge (this is the usual case for S-matrix theory), and in the other class the Hilbert norms diverge. The simplest example of the second case is a plane wave, e.g., $|\rho(0)\rangle\rangle=|\mathbf{k}\rangle\langle\mathbf{k}|$, which is normalized by the Dirac δ function as

$$\langle\langle\mathbf{p};\mathbf{p}'|\rho(0)\rangle\rangle=\delta(\mathbf{p}-\mathbf{p}')\,\delta(\mathbf{p}-\overline{\mathbf{k}}). \tag{2.29}$$

With this initial condition, the interaction is *persistent*. There are no free-in and free-out states. In this situation one cannot apply the S-matrix theory. The density matrix has a δ-function singularity at the diagonal components in momentum representation. For this case the Hilbert norm is proportional to an ill-defined expression $\delta(0)$ [see (2.20)]. In order to avoid this meaningless expression, we can formulate the problem in terms of the box normalization formalism with the volume L^d, then take the limit $L\to\infty$ (see also Sec. III). In this formalism, we can understand that $\delta(\mathbf{k})$ at $\mathbf{k}=0$ is a diverging quantity of order L^M. The box normalization formalism is important in nonequilibrium statistical physics, as this allows for the handling of the thermodynamic limit (i.e., $N\to\infty$, $L\to\infty$ with $c=N/L^d$ finite) [10].

III. TWO-BODY SCATTERING

Let us first consider two-body scattering. For simplicity, we consider a δ-function interaction in one-dimensional configuration space (i.e., $d=1$). Eliminating the center-of-mass motion, the problem of two-body scattering is reduced to a problem of potential scattering for a single particle with the Hamiltonian

$$H=H_0+\lambda V=-\frac{\partial^2}{\partial x^2}+\lambda v_0\delta(x), \tag{3.1}$$

where $v_0>0$ is a constant which characterizes the interaction, and x is the distance between the two particles. We have [for (2.2)]

$$\omega_k=k^2 \tag{3.2}$$

and (for every k and p)

$$\langle p|V|k\rangle = v_0 . \tag{3.3}$$

Let us assume that the initial density matrix is in a pure state given by a wave function $\Psi(0)$,

$$|\rho(0)\rangle\rangle = |\Psi(0)\rangle\langle\Psi(0)| . \tag{3.4}$$

We assume that $\Psi(0)$ is a Gaussian wave packet in momentum representation,

$$\langle k|\Psi(0)\rangle = \delta_\eta(k-\overline{k}), \tag{3.5}$$

where

$$\delta_\eta(l) \equiv \frac{1}{\sqrt{2\pi}\,\eta}\, e^{-l^2/2\eta^2} \tag{3.6}$$

and $1/\eta > 0$ is the size of the wave packet in configuration space. We have

$$\langle \Psi(0)|\Psi(0)\rangle = \frac{1}{2\sqrt{\pi}\,\eta} . \tag{3.7}$$

Moreover, we assume that the wave packet has a sharp peak at the most probable momentum k, i.e.,

$$\eta \ll |\overline{k}| . \tag{3.8}$$

For a small limit of η, we can replace (3.6) by a plane wave

$$\lim_{\eta\to 0} \delta_\eta(k-\overline{k}) = \delta(k-\overline{k}), \tag{3.9}$$

and we have the density matrix

$$\langle\langle k;l|\rho(0)\rangle\rangle \to \delta(k-l)\,\delta(k-\overline{k}), \tag{3.10}$$

which lies outside the Hilbert space [see (3.7)] for $\eta\to 0$.

The spreading time of the wave packet by the free motion is given by $t_s \sim 1/\eta^2$ [3]. We shall always consider time scales where the spreading of the wave packet is negligible, i.e.,

$$t \ll t_s . \tag{3.11}$$

We shall calculate the transition probability for *nonforward* scattering given by the condition

$$|p-\overline{k}| \gg \eta, \tag{3.12}$$

where p is the final momentum.

For a finite size of the wave packet, there is another characteristic time scale, the duration of collision [see (3.30) for the precise definition]

$$\tau_c \sim \frac{1}{\overline{k}\,\eta} . \tag{3.13}$$

We are interested in a comparison between the transition probability after the collision (i.e., the time scale $t \gg \tau_c$) and the one during the collision ($t \ll \tau_c$).

By the resolvent formalism (2.10), the transition probability to the state $|p;p\rangle\rangle$ is given by

$$\langle\langle p;p|\rho(t)\rangle\rangle = \frac{1}{2\pi i}\int_C dz\; e^{-izt}\,\frac{1}{z} \times \langle\langle p;p|[1+\mathscr{T}(z)R_0(z)]|\rho(0)\rangle\rangle . \tag{3.14}$$

For $t>0$ the pole at $z=0$ is located in the first Riemann sheet, as the contour C is located in the upper-half-plane [12]. Hence the evolution for large time scales (i.e., $t \gg \omega_{\overline{k}}^{-1}$) is determined by the residue at $z=+i\epsilon$, with $\epsilon\to 0+$. In order to obtain the transition probability after the collision, we have to take the limit $\epsilon\to 0+$, keeping η finite. Hence for $t \gg \tau_c$ we have

$$\eta|\overline{k}| \gg \epsilon . \tag{3.15}$$

In contrast, if the wave packet is large enough, we can also consider the long-time evolution, but for times shorter than the duration of the collision (i.e., $\tau_c \gg t \gg \omega_{\overline{k}}^{-1}$). For this time scale we can approximate the wave packet by a plane wave, taking the limit $\eta\to 0$ [see (3.9)]. This implies that the limit $\epsilon\to 0+$ should be taken with the condition

$$\eta|\overline{k}| \ll \epsilon . \tag{3.16}$$

This shows that for large wave packets we can consider *two different asymptotic limits*: In the first limit (3.15) one keeps η finite, so that the initial state is in the Hilbert space. On the other hand, if we take the second limit (3.16), then the state is outside the Hilbert space [see (3.9) and (3.10)]. Here we come to the interesting conclusion that *scattering for finite time can be described by the evolution of states outside the Hilbert space*. In Sec. IX we shall discuss the validity of this statement in more detail.

In order to simplify the calculations, we assume that the interaction is weak, i.e., $\lambda \ll 1$. For $v_0>0$ (i.e., a repulsive interaction) we can use the perturbation expansion in powers of λ. We evaluate the transition probability by the lowest order approximation in this series expansion. The extension to a more general case is straightforward using the t-matrix formulation (see Appendix A).

In the perturbation expansion, the dominant contribution to the transition probability for nonforward scattering (3.12) is given by the second-order term λ^2 [see (2.15)]

$$\langle\langle p;p|\rho(t)\rangle\rangle = \frac{\lambda^2}{2\pi i}\int_{-\infty}^{+\infty} dk \int_{-\infty}^{+\infty} dl \int_C dz\; e^{-izt}\,\frac{1}{z}\,\langle\langle p;p|L_V R_0(z) L_V|k;l\rangle\rangle\,\frac{1}{z-w_{kl}}\,\langle\langle k;l|\rho(0)\rangle\rangle + O(\lambda^3). \tag{3.17}$$

The matrix elements of L_V are given by

$$\langle\langle k';l'|L_V|k;l\rangle\rangle = \langle\langle k';l'|(V\times 1 - 1\times V)|k;l\rangle\rangle = v_0\,\delta(l-l') - \delta(k'-k)v_0 . \tag{3.18}$$

This leads to

$$\langle\langle p;p|\rho(t)\rangle\rangle \approx -\frac{\lambda^2}{2\pi i}\int dk\int dl\int_C dz\; e^{-izt}\,\frac{1}{z}\,v_0\left(\frac{1}{z-w_{pl}}+\frac{1}{z-w_{kp}}\right)v_0\,\frac{1}{z-w_{kl}}\,\langle\langle k;l|\rho(0)\rangle\rangle. \tag{3.19}$$

Let us first consider the case $t\gg\tau_c$. This corresponds to the usual situation with which S-matrix theory deals. Taking the residue at $z=+i\epsilon$ of (3.19) we obtain

$$\begin{aligned}\langle\langle p;p|\rho(t)\rangle\rangle &\approx -\lambda^2 v_0^2\int_{-\infty}^{+\infty}dk\int_{-\infty}^{+\infty}dl\left(\frac{1}{i\epsilon-w_{pl}}+\frac{1}{i\epsilon-w_{kp}}\right)\frac{1}{i\epsilon-w_{kl}}\,\langle\langle k;l|\rho(0)\rangle\rangle\\ &= -\lambda^2 v_0^2\int dk\;dl\;\frac{1}{i\epsilon-w_{pl}}\,\frac{1}{i\epsilon-w_{kp}}\left(1+\frac{i\epsilon}{i\epsilon-w_{kl}}\right)\langle\langle k;l|\rho(0)\rangle\rangle.\end{aligned} \tag{3.20}$$

Let us define new variables s and u through the relations

$$k=\overline{k}+\eta s,\quad l=\overline{k}+\eta u. \tag{3.21}$$

Then the initial wave packet (3.4) is written as

$$\langle\langle k;l|\rho(0)\rangle\rangle=\frac{1}{2\pi\eta^2}\,e^{-(s^2+u^2)/2}. \tag{3.22}$$

This shows that the significant contribution to the transition probability comes from the initial density matrix with $|s|$ of order (or less than) 1 in the integration over s (and similarly for u). Using condition (3.8) we can approximate ω_k by

$$\omega_k=\overline{k^2}\left[1+2s\,\frac{\eta}{\overline{k}}+s^2\left(\frac{\eta}{\overline{k}}\right)^2\right]\approx\omega_{\overline{k}}+2\eta\overline{k}s. \tag{3.23}$$

Substituting this into (3.20), we have

$$\langle\langle p;p|\rho(t)\rangle\rangle\approx\lambda^2 v_0^2\int_{-\infty}^{\infty}ds\int_{-\infty}^{\infty}du\;\frac{1}{+i\epsilon+w_{\overline{kp}}+2\eta\overline{k}u}\,\frac{1}{-i\epsilon+w_{\overline{kp}}+2\eta\overline{k}s}\left[1+\frac{i\epsilon}{i\epsilon-2\eta\overline{k}(s-u)}\right]\frac{1}{2\pi}\,e^{-(1/2)(s^2+u^2)}. \tag{3.24}$$

For $t\gg\tau_c$, we can drop the second term inside the bracket [see (3.15)], to obtain

$$\langle\langle p;p|\rho(t)\rangle\rangle\approx\frac{1}{2\pi}\left|\int_{-\infty}^{\infty}ds\;\frac{\lambda v_0}{-i\epsilon+w_{\overline{kp}}+2\eta\overline{k}s}\,e^{-s^2/2}\right|^2. \tag{3.25}$$

The evaluation of the integral in (3.25) is presented in Appendix B. Here we display only the result [see (B7)]:

$$\begin{aligned}\langle\langle p;p|\rho(t)\rangle\rangle\approx{}&\frac{\pi\lambda^2 v_0^2}{2(2\eta\overline{k})^2}\,e^{-w_{kp}^2/(2\eta\overline{k})^2}\\ &\times\left|\mathrm{sgn}(\overline{k})-\frac{2i}{\sqrt{\pi}}\,\mathrm{erfi}\left(\frac{w_{\overline{kp}}}{2\sqrt{2}\,\eta\overline{k}}\right)\right|^2,\end{aligned} \tag{3.26}$$

where $\mathrm{erfi}(x)$ is the imaginary error function [see (B3)]. As one could expect, the transition probability becomes time independent after the collision.

We note that this result, valid for times after the collision, is given by the square of the transition amplitude. This corresponds to the well-known result of the S-matrix theory, which gives us the transition probability (for $t\to+\infty$)

$$\langle\langle p;p|\rho(t)\rangle\rangle\to|\langle\mathbf{p}|\Omega_H(\omega_p+i\epsilon)|\Psi(0)\rangle|^2, \tag{3.27}$$

where Ω_H is the Möller scattering operator associated with the Hamiltonian H [2–4]. Applying this to the second-order contribution corresponding to the process which we are considering, we have

$$\langle\langle p;p|\rho(t)\rangle\rangle\approx\left|\int dk\;\frac{\lambda v_0}{i\epsilon-w_{kp}}\,\langle k|\Psi(0)\rangle\right|^2. \tag{3.28}$$

Using condition (3.8), we see that (3.28) reduces to (3.25).

Equation (3.26) has a sharp peak with a width $\sim\eta|k|$ at the resonance energy $\omega_p=\omega_{\overline{k}}$, and has small corrections in the tail part far from the peak [see (B10) and (B11)]. For small enough η, and for a smooth enough function $f(\omega_p)$ around $\omega_{\overline{k}}$, we can approximate the integration of (3.26) over the final state as (see Appendix C)

$$\int_{\omega_k^{-}-\Delta\omega}^{\omega_k^{-}+\Delta\omega} d\omega_p f(\omega_p)\langle\langle p;p|\rho(t)\rangle\rangle$$

$$\approx f(\omega_{\vec{k}})\int d\omega_p\langle\langle p;p|\rho(t)\rangle\rangle \approx 2\pi\lambda^2 v_0^2\tau_c f(\omega_{\vec{k}}), \tag{3.29}$$

where τ_c is the duration of collision given by (see also Appendix D)

$$\tau_c \equiv \frac{\sqrt{\pi}}{4\eta|\overline{k}|}, \tag{3.30}$$

and the domain of the integration involves the entire contribution from the peak, i.e., $\Delta\omega \gg \eta|\overline{k}|$. Hence we have

$$\langle\langle p;p|\rho(t)\rangle\rangle \approx 2\pi\lambda^2 v_0^2\tau_c\delta(w_{\overline{kp}}). \tag{3.31}$$

[If we consider the case $\Delta\omega \ll \eta|\overline{k}|$, the asymptotic expansion of the imaginary error function leads for (3.26) [see (B10) and (3.6)] to

$$\langle\langle p;p|\rho(t)\rangle\rangle \approx \pi\lambda^2 v_0^2\tau_c\delta_{\sqrt{2}\eta\overline{k}}(w_{\overline{kp}}),$$

which is different from (3.31) by factor 2 for $\eta\to 0$. As this formula does not involve a significant contribution around the peak, this is not a consistent approximation. Instead, we should use (3.31).] The dominant contribution thus comes from the process that preserves the unperturbed energy between the initial and the final states. Because the contribution comes from the small denominator at the resonance point $w_{p\overline{k}}=0$ [see the discussion below (3.36)], we may call the energy-conserving process the on-resonance-shell process (or the on-shell process, for short). Conversely, we call the case

$$|w_{\overline{kp}}| \gg \eta|\overline{k}| \tag{3.32}$$

the off-resonance-shell process (or the off-shell process, for short).

We now focus on the off-shell process. This process is much smaller than the resonance contribution for two-body scattering. However, as we shall now show, there is an interesting discrepancy in the off-shell process between the two asymptotic descriptions. With condition (3.32), and using (B11), we can approximate (3.26) by

$$\langle\langle p;p|\rho(t)\rangle\rangle \approx \frac{\lambda^2 v_0^2}{w_{\overline{kp}}^2}. \tag{3.33}$$

Next let us consider the case $t \ll \tau_c$, i.e., the situation during collision (3.16). For this case we can approximate the initial wave packet by a plane wave with $\eta\to 0$. Then from (3.19) we obtain

$$\langle\langle p;p|\rho(t)\rangle\rangle \approx -\frac{\lambda^2 v_0^2}{2\pi i}\int_C dz\,\frac{e^{-izt}}{z^2}\left(\frac{1}{z-w_{\overline{kp}}}+\frac{1}{z+w_{\overline{kp}}}\right). \tag{3.34}$$

Again, the residue of (3.34) at $z=+i\epsilon$ dominates for large t. Neglecting the contributions other than the residue at $z=+i\epsilon$, we obtain

$$\langle\langle p;p|\rho(t)\rangle\rangle \approx \lambda^2 v_0^2 2\pi t\,\delta(w_{\overline{kp}}) + \lambda^2 v_0^2\left[\frac{1}{(w_{\overline{kp}}+i\epsilon)^2} + \frac{1}{(w_{\overline{kp}}-i\epsilon)^2}\right], \tag{3.35}$$

where we have used the relation

$$2\pi i\,\delta(w) = \lim_{\epsilon\to 0+}\left(\frac{1}{w-i\epsilon}-\frac{1}{w+i\epsilon}\right) = \lim_{\epsilon\to 0+}\frac{2i\epsilon}{w^2+\epsilon^2}. \tag{3.36}$$

Equation (3.35) is the expression we have to compare with (3.26). In this expression there appears a secular term proportional to t. As indicated in (3.36), the secular effect comes from the zero in the denominator. This corresponds to Poincaré's resonance.

As a result of the secular effect, the on-resonance-shell process dominates for large t. Then we obtain (during the collision with large enough wave packets)

$$\langle\langle p;p|\rho(t)\rangle\rangle \approx 2\pi\lambda^2 v_0^2 t\,\delta(w_{\overline{kp}}). \tag{3.37}$$

Combining this result with (3.31), we see that the transition probability during the collision grows linearly in time, then reaches a constant after the collision. The on-shell process is smoothly connected during and after the collision.

We now show that this is not the case for the off-resonance-shell process. With condition (3.32), from (3.35) we obtain (for the off-shell part during the collision)

$$\langle\langle p;p|\rho(t)\rangle\rangle \approx 2\frac{\lambda^2 v_0^2}{w_{\overline{kp}}^2}. \tag{3.38}$$

Note the factor 2 in this expression, which is different from (3.33).

This shows that the tail contribution in the transition probability during the collision differs from the one after the collision. As the tail contribution for two-body scattering does not appear in the secular term, this contribution is negligible for long-time scales, as compared with the on-resonance-shell part. However, as we shall see in detail in Sec. VII, a similar difference between the situations during and after the collision appears even in the secular term for three-body scattering. This then leads to a non-negligible effect in the three-body scattering cross section. Therefore, it is worthwhile to have a closer look at the origin of this difference for two-body scattering. To this end, let us again consider (3.24). With condition (3.32), we can approximate (3.24) by

$$\langle\langle p;p|\rho(t)\rangle\rangle \approx \frac{\lambda^2 v_0^2}{w_{\overline{kp}}^2}\int_{-\infty}^{\infty} ds\int_{-\infty}^{\infty} du\left[1+\frac{i\epsilon}{i\epsilon-2\eta\overline{k}(s-u)}\right] \times\frac{1}{2\pi}\,e^{-(1/2)(s^2+u^2)}. \tag{3.39}$$

In this expression, there appear two small quantities ϵ and η. The value of this expression depends on the way the asymptotic limits (3.15) or (3.16) are taken. The first asymptotic is the limit $\epsilon\to 0+$, keeping η finite. Then the second

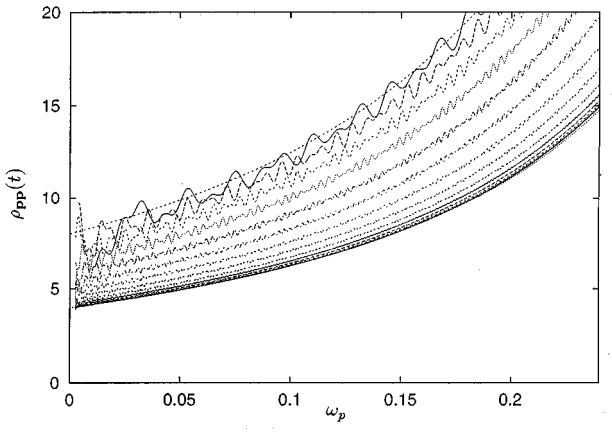

FIG. 1. The tail part (i.e., the off-resonance part) of the line shape of the transition probability for two-body scattering as a function of the final energy w_p, for different times, showing the shift from during (upper line) to after the collision (lower line; see text).

term inside the bracket of (3.39) vanishes. This corresponds to the case after the collision. We then recover the result (3.33) as

$$\langle\langle p;p|\rho(t)\rangle\rangle \approx \frac{\lambda^2 v_0^2}{w_{kp}^2}\frac{1}{2\pi}\left|\int_{-\infty}^{\infty} ds\ e^{-s^2/2}\right|^2 = \frac{\lambda^2 v_0^2}{w_{kp}^2}. \tag{3.40}$$

For the second asymptotic, we take the limit $\eta \to 0$ first, and take the limit $\epsilon \to 0+$ later. Then the term $2\eta k(s-u)$ in the denominator in the second term in the bracket of (3.39) is negligible as compared with ϵ. This corresponds to the case during the collision [see (3.16)]. We then recover result (3.38) as

$$\langle\langle p;p|\rho(t)\rangle\rangle \approx \frac{\lambda^2 v_0^2}{w_{kp}^2}\,2\,\frac{1}{2\pi}\left|\int_{-\infty}^{\infty} ds\ e^{-s^2/2}\right|^2 = 2\,\frac{\lambda^2 v_0^2}{w_{kp}^2}. \tag{3.41}$$

The first asymptotic corresponds to the case of *transient* processes. As η is finite, the density matrix has a finite Hilbert norm defined by (2.19). The evolution can be described in the Hilbert space. On the other hand, the second asymptotic corresponds to the case of *persistent* processes.

In summary, we have seen that the off-shell part of the transition probability after the collision differs from the one during the collision (the former is two times larger than the latter). The line shapes are different between after and during the collision. This difference is small as it appears only in the tail contribution, and does not make any significant contribution to the two-body scattering cross section. However, for three-body scattering this difference becomes significant, because it becomes of the same order of magnitude as the genuine three-body transition probability. We shall show this in the subsequent sections.

We have verified the above predictions by a numerical calculation of the transition probability. In Fig. 1 we display the result. We have generated this result by taking the square of the numerical integration of

$$\begin{aligned}\lambda\langle p|\Psi_1(t)\rangle &= \int dk\ \frac{\lambda v_0}{\omega_p-\omega_k+i\epsilon}\,(e^{-i\omega_p t}-e^{-i\omega_k t})\langle k|\Psi(0)\rangle \\ &= -2i\lambda v_0 e^{+i\omega_p t/2}\int dk\ \frac{\sin[(\omega_p-\omega_k)t/2]}{\omega_p-\omega_k} \\ &\quad\times e^{+i\omega_k t/2}\langle k|\Psi(0)\rangle. \end{aligned}\tag{3.42}$$

Here $|\Psi_1(t)\rangle$ is the first-order contribution of the Dyson series, i.e.,

$$|\Psi(t)\rangle = |\Psi_0(t)\rangle + \lambda|\Psi_1(t)\rangle + \lambda^2|\Psi_2(t)\rangle + \cdots, \tag{3.43}$$

which is obtained by the iteration of the integral equation for the Hamiltonian [cf. (2.8)]

$$e^{-iHt} = e^{-iHt} - i\lambda\int_0^t dt' e^{-iH_0(t-t')}Ve^{-iHt'}. \tag{3.44}$$

To obtain the first equality in (3.42), we have added the infinitesimal $i\epsilon$ in the denominator, as the contribution at $\omega_p=\omega_k$ is finite for $\epsilon=0$ and the integrand has no discontinuity at $\epsilon=0$ as a function of ϵ.

In order to perform the numerical integration of (3.42), we have replaced the continuous spectrum of k by the discrete spectrum (with integers n and $\Delta k \equiv 2\pi/L$)

$$k = n\Delta k, \tag{3.45}$$

by putting the system in a box of size L with the usual periodic boundary conditions. For large enough L, we can replace the integration over k by its summation as

$$\int dk \Rightarrow \Delta k \sum_k . \tag{3.46}$$

As a result of the discretization, there appears a characteristic time scale $t_B \sim 1/(|k|L)$ which is a crossing time from one side of the box to the other side with a typical momentum k. The time scale t of our observation should be chosen with the condition

$$t \ll t_B. \tag{3.47}$$

Moreover, in order to deal with distributions [such as (3.36)] in summations, we have to choose the value of ϵ as (see Appendix E)

$$\frac{|dw_k/dk|\Delta k}{\epsilon} \ll 1. \tag{3.48}$$

In the numerical integration for the time scale during the collision, there appear contributions which oscillate rapidly for large times as a function of ω_p. They correspond to the pole contributions in the integration of (3.34) over z other than the pole at $z=+i\epsilon$. For large time scales the contributions approach zero in the sense of distribution (e.g., in the integration over the final state p with a suitable test function). Hence, to compare the numerical simulation to our prediction, we have taken averages of the numerical results over the final momentum with intervals involving a few periods of these rapid oscillations.

In Fig. 1, we display the numerical results for the tail part (i.e., the off-shell part) of the transition probability as a function of ω_p for several time scales. The results are for the case $w_{\bar{k}}=1.0$, $\eta=4.0\times10^{-4}$, and $\lambda v_0=1.0$. For these parameters we have $\tau_c=1107.8$ [see (3.30)]. In this figure the upper dashed line is the theoretical result (3.41) for $t\ll\tau_c$, while the lower dashed line is the theoretical result (3.40) for $t\gg\tau_c$. The wavy lines in between these two are generated by numerical integration of (3.42). From upper to lower they correspond to $t=0.1\tau_c$, $0.3\tau_c$,... up to $2.1\tau_c$. In agreement with the theoretical prediction, the numerical results shift from the theoretical result for $t\ll\tau_c$ to the theoretical result derived from the S-matrix approach for $t\gg\tau_c$.

IV. THREE-BODY SCATTERING

We now consider our main problem: three-body scattering. For simplicity, we consider a δ-function interaction in a one-dimensional configuration space. For the S-matrix regime, with the wave function in Hilbert space, this system is exactly solvable [13–15]. However, for the asymptotic situation in the statistical mechanics approach, the system becomes nonintegrable. We shall discuss this in detail in a separate paper [16]. We assume the three particles have the same mass $m=\frac{1}{2}$, and that the Hamiltonian is given by

$$H=-\sum_{a=1}^{3}\frac{\partial^2}{\partial R_a^2}+\sqrt{2}\lambda\sum_{a<b}^{3}v_{ab}\delta(R_a-R_b), \tag{4.1}$$

where R_a is the position of particle a, and v_{ab} is a constant which characterizes the interaction between particles a and b. We shall also use the standard notation $v_c\equiv v_{ab}$, where (a,b,c) are chosen cyclically from (1,2,3) such as $v_3=v_{12}$. We introduce the factor $\sqrt{2}$ in order to have a more compact expression for the matrix elements of the interaction, written in the Jacobi coordinate representation. We assume $v_c>0$, so that there are no bound states. Moreover, we assume the interaction is weak. Hence we can evaluate the transition probability of scattering in the lowest order approximation in the perturbation expansion in λ. For the repulsive interaction, which we consider in this paper, the extension to arbitrary order in λ is straightforward using the t-matrix formulation (see Appendix A).

In the center-of-mass system, we have

$$K_1+K_2+K_3=0, \tag{4.2}$$

where K_i are the unperturbed momenta. Because the three particles have the same mass, the sum $R_1+R_2+R_3$ is proportional to the position of the center of mass. We put

$$R_1+R_2+R_3=0. \tag{4.3}$$

We now introduce Jacobi's coordinates [5] defined by

$$k_{xa}=\frac{K_b-K_c}{\sqrt{2}},\quad r_{xa}=\frac{R_b-R_c}{\sqrt{2}},$$
$$k_{ya}=\sqrt{\tfrac{3}{2}}K_a,\quad r_{ya}=\sqrt{\tfrac{3}{2}}R_a, \tag{4.4}$$

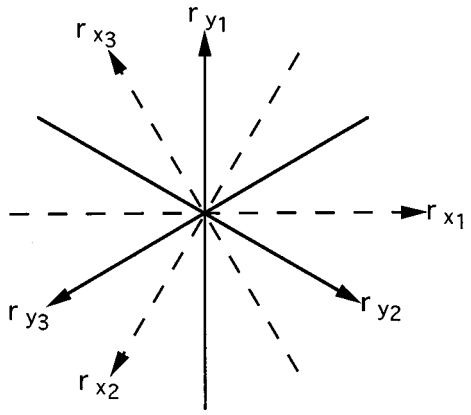

FIG. 2. The three Jacobi coordinate systems. The solid lines correspond to the walls.

where (a,b,c) are chosen cyclically from (1,2,3), as before. The unperturbed energy can be written, for any $a=1$, 2, or 3, as (see Appendix F)

$$\omega_k\equiv\sum_{i=1}^{3}K_i^2=k_{xa}^2+k_{ya}^2. \tag{4.5}$$

In Appendix F we show that the three sets of Jacobi variables are related by a rotation with the angle $\phi_0\equiv2\pi/3$ (see Fig. 2)

$$\begin{pmatrix}r_{xa}\\ r_{ya}\end{pmatrix}=\begin{pmatrix}\cos\phi_0 & \sin\phi_0\\ -\sin\phi_0 & \cos\phi_0\end{pmatrix}\begin{pmatrix}r_{xb}\\ r_{yb}\end{pmatrix}, \tag{4.6}$$

as well as

$$\begin{pmatrix}k_{xa}\\ k_{ya}\end{pmatrix}=\begin{pmatrix}\cos\phi_0 & \sin\phi_0\\ -\sin\phi 0 & \cos\phi_0\end{pmatrix}\begin{pmatrix}k_{xb}\\ k_{yb}\end{pmatrix}, \tag{4.7}$$

where a and b are chosen cyclically from (1,2,3), as before. Therefore, the variables (r_{xa},r_{ya}) and (k_{xa},k_{ya}) are components of vectors $\mathbf{r}$ and $\mathbf{k}$ in the ath coordinate system, respectively:

$$\mathbf{r}\equiv(r_{xa},r_{ya}),\quad \mathbf{k}\equiv(k_{xa},k_{ya}). \tag{4.8}$$

The magnitude of these vectors is invariant under the change of coordinate systems. For example, the magnitude of $\mathbf{k}$ is equal to the square root of the kinetic energy [see (4.5)].

After eliminating the total momentum, the Hamiltonian (4.1) can be written in terms of Jacobi's coordinates as

$$H=H_0+\lambda V=-\frac{\partial^2}{\partial r_{xa}^2}-\frac{\partial^2}{\partial r_{ya}^2}+\lambda\sum_{c=1}^{3}v_c\delta(r_{xc}). \tag{4.9}$$

We can interpret (4.9) as the Hamiltonian that represents the evolution of a single particle in two-dimensional space, interacting with three walls [17]. The three walls are located at $r_{xc}=0$ (i.e., the r_{yc} axis), for $c=1$, 2, and 3, respectively. We indicate the walls by the solid lines in Fig. 2.

The eigenstates of H_0 are plane waves with momenta $\mathbf{k}$ given by

$$H_0|\mathbf{k}\rangle=\omega_k|\mathbf{k}\rangle \tag{4.10}$$

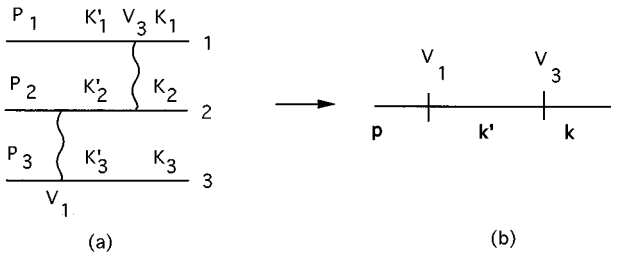

FIG. 3. (12)–(23) collision process: (a) original representation, (b) representation with Jacobi momenta.

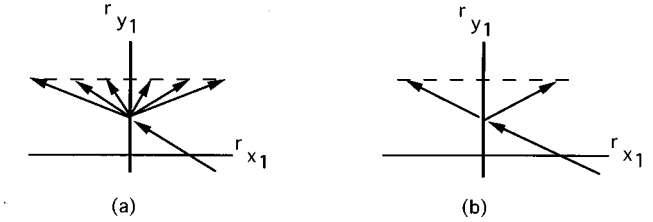

FIG. 4. (a) Off-shell and (b) on-shell collisions of the particle with a wall.

They satisfy

$$\int d^2k|\mathbf{k}\rangle\langle\mathbf{k}| = 1,$$

$$\langle\mathbf{p}|\mathbf{k}\rangle = \delta(\mathbf{p}-\mathbf{k}) = \delta(p_{xa}-k_{xa})\,\delta(p_{ya}-k_{ya}). \quad (4.11)$$

The momentum representation of the interaction $V_a \equiv v_a\delta(r_{xa})$ is given by

$$\langle\mathbf{p}|V_a|\mathbf{k}\rangle = v_a\delta(p_{ya}-k_{ya}). \quad (4.12)$$

Equation (4.12) corresponds to a collision between particles b and c, while particle a is moving freely [see (4.4)].

Similar to two-body scattering, let us assume that the initial density matrix is given by

$$|\rho(0)\rangle\rangle = |\Psi(0)\rangle\langle\Psi(0)|, \quad (4.13)$$

with a Gaussian packet in the momentum representation [see (3.6)]

$$\langle\mathbf{k}|\Psi(0)\rangle = \delta_\eta(\mathbf{k}-\overline{\mathbf{k}}) \equiv \delta_\eta(k_{x1}-\overline{k_{x1}})\,\delta_\eta(k_{y1}-\overline{k_{y1}}). \quad (4.14)$$

Again, we assume that the wave packet has a sharp peak at the most probable momentum $\mathbf{k}$, i.e.,

$$\eta \ll |\overline{\mathbf{k}}|. \quad (4.15)$$

Similar to Sec. III, we shall calculate the transition probability for nonforward scattering given by the condition

$$|\mathbf{p}-\overline{\mathbf{k}}| \gg \eta, \quad (4.16)$$

where $\mathbf{p}$ is the final momentum.

V. DISTRIBUTION OF FINAL MOMENTA

We focus our attention on the lowest order term in λ that involves all three particles. We consider a collision between particles 1 and 2 followed by a collision between particles 2 and 3. This process is of order λ^2 in wave-function space, and can be schematically written by a diagram as shown in Fig. 3. Following Faddeev, we can resum the processes in three-body scattering in terms of the two-body t matrix. [18] Considering all connected diagrams we can easily extend our result to an arbitrary order in the coupling constant λ. See Appendix A.

Diagram (a) in Fig. 3 represents the transition in the original coordinate system. This corresponds to a transition from the initial state (K_1,K_2,K_3) to the final state (P_1,P_2,P_3), going through the intermediate state (K_1',K_2',K_3') in wave-function space. Diagram (b) shows the same process as in diagram (a) but in Jacobi's coordinate system. This represents the transition from the initial state $\mathbf{k}\equiv(k_{x_a},k_{y_a})$ to the final state $\mathbf{p}\equiv(p_{x_a},p_{y_a})$, through the intermediate state $\mathbf{k}'\equiv(k'_{x_a},k'_{y_a})$.

In Sec. III we classified the transition probability for two-body scattering according to on-resonance processes, as well as off-resonance processes. On-resonance processes make dominant contributions, as they lead to secular effects which grow in time during the collision. This classification is also essential to understanding three-body collisions. Without going into any complicated calculations, we may already predict the results for the transition probability using this classification. In order to show this, let us discuss the geometrical meaning of on- and off-resonance processes.

As mentioned in Sec. IV, (4.9) can be interpreted as the Hamiltonian of a single particle in a two-dimensional space, interacting with three walls. Let us consider the interaction of the particle with the wall located at $r_{x1}=0$. Equation (4.12) with $a=1$ describes this interaction. Since it corresponds to a collision between particles 2 and 3, while particle 1 moves without any disturbance, the y_1 component of the momentum does not change after the particle hits the wall, i.e., $p_{y1}=k_{y1}$. Hence, if there is no other restriction, the momenta after the collision with this wall will line up parallel to the r_{x1} axis [see Fig. 4(a)].

In addition, if the unperturbed energy is conserved as $\omega_k=\omega_p$, i.e., if the process is on-resonance-shell, we have

$$k_{x1}^2+k_{y1}^2 = p_{x1}^2+p_{y1}^2, \quad (5.1)$$

which leads to

$$p_{x1} = \pm k_{x1}. \quad (5.2)$$

Thus there is a reflected particle, as well as a transmitted particle. The horizontal component of the momentum p_{x1} (which is proportional to the relative momentum of particles 2 and 3) can only take the same or the opposite sign of its initial value [see Fig. 4(b)].

Now we can draw the final momentum distribution of the

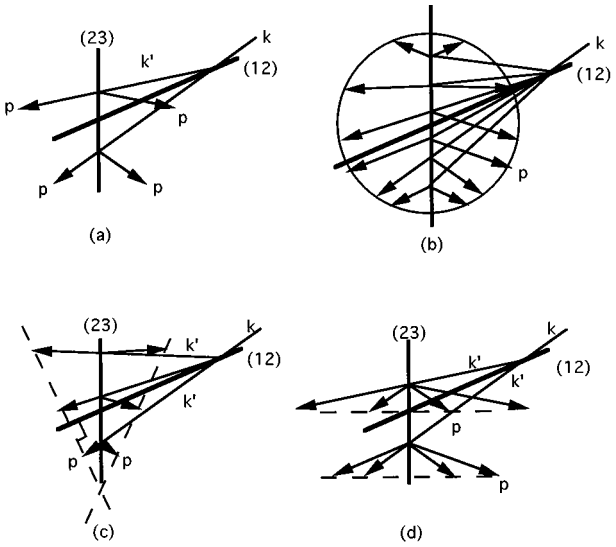

FIG. 5. Interaction processes with the (12) and (23) walls, containing at least one on-shell collision: (a) on-on shell (rescattering), (b) triple collision, (c) on-off shell, and (d) off-on shell (see text).

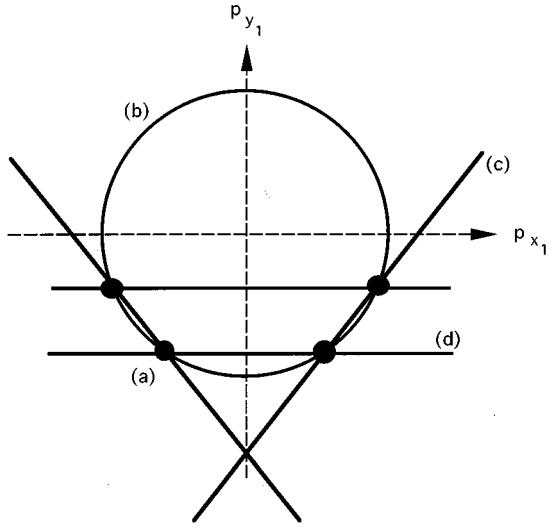

FIG. 6. Final distribution of the momentum for a succession of a (12) interaction followed by a (23) interaction, for time scales shorter than the duration of the collision. The initial momentum is at the lower left dot on the circle. The contributions are (a) rescattering (four dots), (b) triple collision (circle), (c) on-off shell process (tilted lines), and (d) off-on shell process (horizontal lines).

transition probability corresponding to the process in Fig. 3(b). In Fig. 5, we show the processes which contain at least one on-resonance-shell scattering.

Diagram (a) in Fig. 5 corresponds to the process in which the unperturbed energy is preserved between the initial and final states, as well as between the intermediate and final states. We call this process the on-on shell process. This is the process corresponding to rescattering, i.e., to two successive two-body collisions on the resonance shell [6,19]. The first collision splits the incoming beam into two (transmitted and reflected) beams. Then the second collision again splits each beam into two. Hence there are four possible peaks in the distribution of the final momenta. Note that the lower left position of the arrow in this diagram has the same direction as the incoming beam. This corresponds to forward scattering.

Diagram (b) corresponds to the process in which the unperturbed energy is preserved between the initial and final states, but not in the intermediate state. Therefore, there must be a very short-time interval between the two collisions. In other words, the three particles interact nearly at the same point in space. We may call this process the genuine triple collision (or the triple collision, in short). The collision with each wall is an off-shell process. But, since the final unperturbed energy is equal to the initial unperturbed energy, the final momentum distribution is a circumference [see (4.5)] that has a radius p_r equal to the square root of the conserved energy, i.e., $p_r=\sqrt{\omega_k}$.

Diagram (c) corresponds to the process in which the unperturbed energy is preserved between the final and intermediate states, but not between the intermediate and initial states. We may call this process the on-off shell process. The beam scattered by the first off-shell interaction is lined up on the left tilted dashed line [which is perpendicular to the (12) wall as shown in Fig. 5(c)]. The second interaction is on-resonance-shell. Then this produces two dashed lines. One corresponds to the transmitted beams, and the other to their reflections.

Finally, diagram (d) is the off-on shell process. This corresponds to the process in which the unperturbed energy is not preserved between the final and intermediate states, but is preserved between the intermediate and initial states. The first on-shell interaction splits the incoming beam into two beams; one is a transmitted beam and the other a reflected beam. Then, after the second off-shell interaction, these beams are both lined up on the two horizontal dashed lines shown in Fig. 5(d).

In Fig. 6 we sketch the total results of the momentum distribution in Jacobi's coordinate plane during the collision. As has been shown in Sec. III, there is a process appearing only at intermediate times in two-body scattering. A similar phenomenon also exists in three-body scattering. We shall show in Sec. VI that the off-on shell process is transient, and can be observed only during the collision. In Fig. 7 we sketch the momentum distribution after all interaction processes are terminated in accordance with the S-matrix approach. The difference between this momentum distribution and the previous one is quite significant.

VI. DIAGRAMMATIC REPRESENTATION IN LIOUVILLE SPACE

In this section and Sec. VII we shall verify the existence of the transient phenomenon mentioned in Sec. V in terms of the resolvent formalism. The calculations are quite parallel to the ones performed in Sec. III for two-body scattering. To perform the calculation systematically, we shall introduce a diagrammatic representation of the perturbation series of the resolvent for (2.16) in the Liouville space.

The interaction L_V consists of two terms, $V\times 1$ and $-1\times V$ [see (2.27)]. In order to describe a collision process

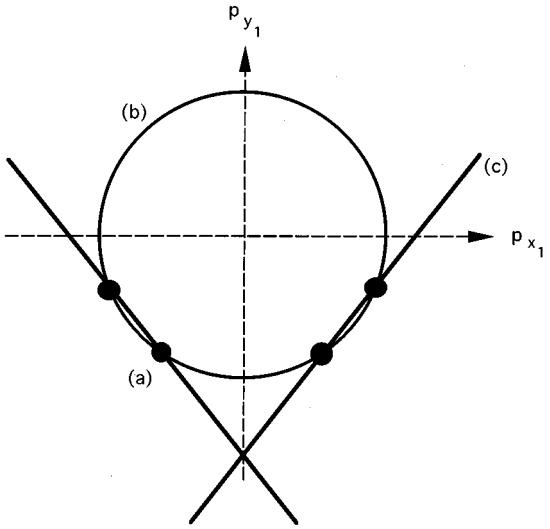

FIG. 7. Final distribution of the momentum for a succession of a (12) interaction followed by a (23) interaction, for time scales larger than the duration of the collision (the S-matrix regime). There are no horizontal lines, which correspond to the off-on shell process.

in the Liouville space schematically, we associate Fig. 8(a) with $V_a\times 1$ and Fig. 8(b) with $-1\times V_a$ (we use the Jacobi coordinate representation).

Figure 8(a) corresponds to the matrix elements

$$\langle\langle \mathbf{k}';\boldsymbol{l}'|(V_a\times 1)|\mathbf{k};\boldsymbol{l}\rangle\rangle=\langle \mathbf{k}'|V_a|\mathbf{k}\rangle\,\delta(\boldsymbol{l}-\boldsymbol{l}'), \tag{6.1}$$

while Fig. 8(b) corresponds to

$$\langle\langle \mathbf{k}';\boldsymbol{l}'|(-1\times V_a)|\mathbf{k};\boldsymbol{l}\rangle\rangle=-\,\delta(\mathbf{k}'-\mathbf{k})\langle \boldsymbol{l}|V_a|\boldsymbol{l}'\rangle. \tag{6.2}$$

Note the relation of the order of the indexes $\boldsymbol{l}'$ and $\boldsymbol{l}$ of diagram (b) to the order of these in the matrix element $\langle \boldsymbol{l}|V_a|\boldsymbol{l}'\rangle$.

Moreover, we can associate the propagator $(z-L_0)^{-1}$ to the two horizontal lines in the diagram, e.g., the lines with indices $\mathbf{k}$ and $\boldsymbol{l}$ in the diagrams in Fig. 8 correspond to

$$\langle\langle \mathbf{k};\boldsymbol{l}|\,\frac{1}{z-L_0}\,|\mathbf{k};\boldsymbol{l}\rangle\rangle=\frac{1}{z-w_{kl}}, \tag{6.3}$$

where the subscript k in w_{kl} is associated with the upper line in the diagram, and l with the lower line. The diagrams in Fig. 8 correspond to the first-order contribution of λ in the perturbation series (2.16). In Figs. 9–11, we display the first few diagrams of the lowest orders. Figure 9 corresponds to the second order, Fig. 10 to the third order, and Fig. 11 the

FIG. 8. Diagramatic representation of the interactions in Liouville space: (a) $V_a\times 1$, (b) $-1\times V_a$.

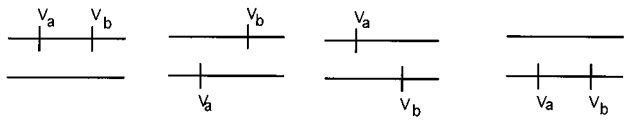

FIG. 9. Second-order diagrams in Liouville space.

first few diagrams of the fourth order. These diagrams consist of many different types of processes: For example, if the indices of the interactions are the same, i.e., $a=b=\cdots$, the processes correspond to the so-called disconnected two-body processes that describe two-body scattering among the three particles in which one of the particles does not participate in the scattering [18]. Three-body scattering is associated with interacting processes with more than one index. Moreover, for a given initial state $|\mathbf{k};\mathbf{k}\rangle\rangle$, these diagrams consist of forward scattering (i.e., the final momenta of all three particles are the same as their initial values), partially forward scattering (i.e., in the final state one of the particles keeps the same momentum as its initial value), and true three-body nonforward scattering (i.e., the final momenta of all three particles change their values of the initial momenta). In the following discussion, we shall restrict ourselves to the true three-body nonforward scattering process. This restricts the number of the diagrams, and simplifies the calculation. The following calculation can be easily extended to the processes including forward and partially forward scattering.

Through the diagrammatic representation, one can easily recognize that the lowest order contributions to the true three-body nonforward scattering process start with λ^4 and are represented by the diagrams in the last line in Fig. 11. Let us consider the case $a=c$ and $b=d$ with $a\neq b$ in the diagrams. These are the simplest processes that lead to the rescattering anomaly for the transition probability in the usual approach by the S-matrix theory. We shall come back this problem below.

In Fig. 12 we show all possible processes for $a=1$ and $b=3$. They correspond to the process in Fig. 3(b) in wave-function space. Each diagram corresponds to different orderings of the interactions $V_1\times 1$, $-1\times V_1$, $V_3\times 1$, and $-1\times V_3$. Replacing V_a by the two-body t matrix $t_a(z)$ with a suitable argument z, one can obtain the corresponding diagram in the Faddeev expansion (see Appendix A). These processes (and the processes obtained by permutation of particles) are the only true three-body nonforward scattering processes that

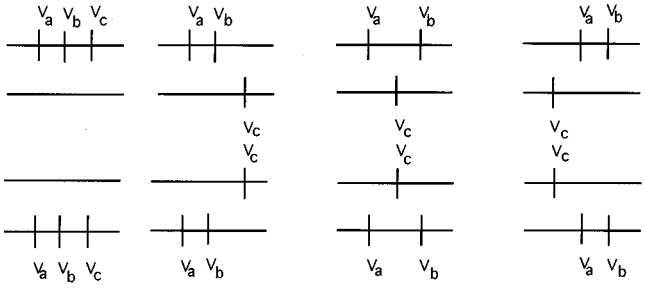

FIG. 10. Third-order diagrams in Liouville space.

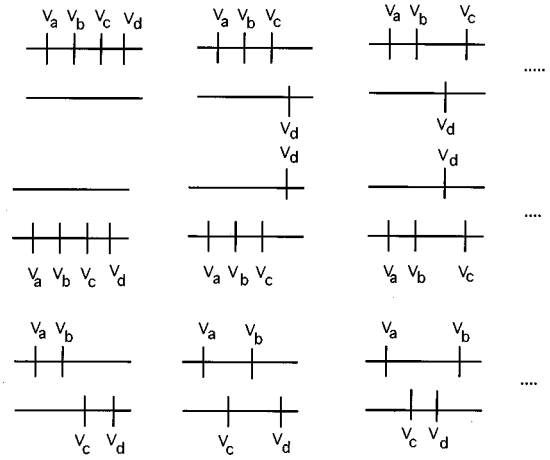

FIG. 11. Some of the fourth-order diagrams in Liouville space.

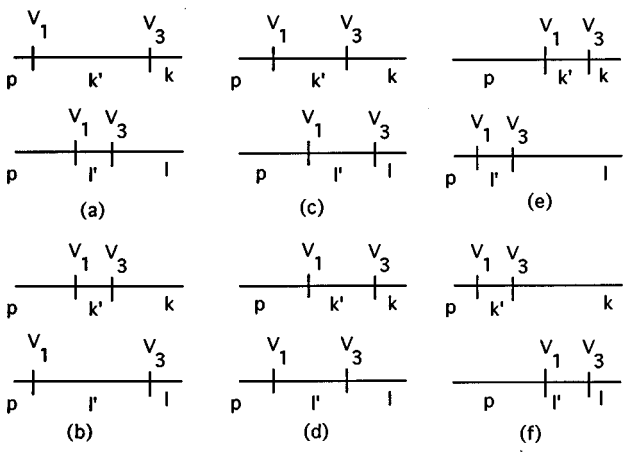

FIG. 12. Fourth-order diagrams in Liouville space corresponding to the process in Fig. 3(b) in wave-function space.

lead to the rescattering anomaly in the usual S-matrix theory approach [6–8]. The momenta $\mathbf{k}$ and $\boldsymbol{l}$ in the diagrams correspond to the density matrix $\rho_{\mathbf{k}\boldsymbol{l}}(0)$.

Diagram (f) represents the term

$$\lambda^4 \frac{1}{z-w_{pp}} \langle \mathbf{p}|V_1|\mathbf{k}'\rangle \frac{1}{z-w_{k'p}} \langle \mathbf{k}'|V_3|\mathbf{k}\rangle \frac{1}{z-w_{kp}} \times \langle \boldsymbol{l}'|(-V_1)|\mathbf{p}\rangle \frac{1}{z-w_{kl'}} \langle \boldsymbol{l}|(-V_3)|\boldsymbol{l}'\rangle \frac{1}{z-w_{kl}}. \quad (6.4)$$

We have $w_{pp}=0$ in the leftmost propagator. Using (4.12), (6.4) can be written as

$$\frac{1}{z} v_1 \delta(k'_{y1}-p_{y1}) \frac{1}{z-w_{k'p}} v_3 \delta(k'_{y3}-k_{y3}) \frac{1}{z-w_{kp}} \times (-v_1)\delta(l'_{y1}-p_{y1}) \frac{1}{z-w_{kl'}} (-v_3)\delta(l'_{y3}-l_{y3}) \frac{1}{z-w_{kl}}. \quad (6.5)$$

Similarly we can write corresponding expressions to diagrams (a)–(e) in Fig. 12. Let us denote the sum of the contributions corresponding to all diagrams of Fig. 12 by $\Phi(\mathbf{k}',\boldsymbol{l}',\boldsymbol{k},\boldsymbol{l},z)$. Then we obtain

$$\Phi(\mathbf{p},\mathbf{k}',\boldsymbol{l}',\mathbf{k},\boldsymbol{l},z)=\lambda^4 v_1^2 v_3^2 \Delta(\mathbf{p},\mathbf{k}',\boldsymbol{l}',\mathbf{k},\boldsymbol{l}) \left[\frac{1}{z} \left(\frac{1}{z-w_{pl'}} + \frac{1}{z-w_{k'p}} \right) \frac{1}{z-w_{k'l'}} \left(\frac{1}{z-w_{k'l}} + \frac{1}{z-w_{kl'}} \right) \frac{1}{z-w_{kl}} + \frac{1}{z} \left(\frac{1}{z-w_{pl'}} \frac{1}{z-w_{pl}} \frac{1}{z-w_{k'l}} + \frac{1}{z-w_{k'p}} \frac{1}{z-w_{kp}} \frac{1}{z-w_{kl'}} \right) \frac{1}{z-w_{kl}} \right], \quad (6.6)$$

where

$$\Delta(\mathbf{p},\mathbf{k}',\boldsymbol{l}',\mathbf{k},\boldsymbol{l}) \equiv \delta(k'_{y1}-p_{y1})\delta(k'_{y3}-k_{y3})\delta(l'_{y1}-p_{y1}) \times \delta(l'_{y3}-l_{y3}). \quad (6.7)$$

The first term inside the brackets [i.e., the term with the propagator $(z-w_{k'l'})^{-1}$] is the sum of diagrams (a)–(d), and the second term is the sum of diagrams (e) and (f). Then the probability density of finding the momentum at $\mathbf{p}$ is given by [see (2.16)]

$$\langle\langle \mathbf{p};\mathbf{p}|\overline{\rho(t)}\rangle\rangle = \int d^2k' \int d^2l' \int d^2k \int d^2l \frac{1}{2\pi i} \times \int_C dz\, e^{-izt} \Phi(\mathbf{p},\mathbf{k}',\boldsymbol{l}',\mathbf{k},\boldsymbol{l},z) \times \langle\langle \mathbf{k};\boldsymbol{l}|\overline{\rho(0)}\rangle\rangle, \quad (6.8)$$

where the bar denotes the process we are looking at. The asymptotic transition probability is given by the residue of (6.8) at the pole $z=+i\epsilon$, i.e.,

$$\langle\langle \mathbf{p};\mathbf{p}|\overline{\rho(t)}\rangle\rangle \approx \int d^2k' \int d^2l' \int d^2k \int d^2l \times \mathrm{Res}_{z=+i\epsilon}[e^{-izt}\Phi(\mathbf{p},\mathbf{k}',\boldsymbol{l}',\mathbf{k},\boldsymbol{l},z) \times \langle\langle \mathbf{k};\boldsymbol{l}|\rho(0)\rangle\rangle], \quad (6.9)$$

where Res ≡ residue. Corresponding to (3.21), let us define the variables $\mathbf{s}$ and $\mathbf{u}$ through the relations

$$\mathbf{k}=\overline{\mathbf{k}}+\eta\mathbf{s}, \quad \boldsymbol{l}=\overline{\mathbf{k}}+\eta\mathbf{u}. \quad (6.10)$$

Then the initial wave packet (4.13) is written as

$$\langle\langle \mathbf{k};\boldsymbol{l}|\rho(0)\rangle\rangle = \frac{1}{2\pi\eta^2} e^{-(|\mathbf{s}|^2+|\mathbf{u}|^2)/2}. \quad (6.11)$$

Corresponding to (3.23), we have (for large wave packet)

$$\omega_k \equiv |\mathbf{k}|^2 = \omega_{\overline{k}} + 2\,\eta(\overline{\mathbf{k}}\cdot\mathbf{s}) + \eta^2|\mathbf{s}|^2 \approx \omega_{\overline{k}} + 2\,\eta(\overline{\mathbf{k}}\cdot\mathbf{s}), \tag{6.12}$$

where we used (4.15). For the energy $\omega_{k'}$ of the intermediate state we have

$$\omega_{k'} = k'^2_{x1} + k'^2_{y1}. \tag{6.13}$$

The δ function in the leftmost interaction $\langle \mathbf{p}|V_1|\mathbf{k}'\rangle$ in the upper line of the diagrams in Fig. 12 leads to [see (4.12)]

$$k'_{y1} = p_{y1}. \tag{6.14}$$

From (4.2) and (4.4), and by the δ function in the rightmost interaction $\langle \mathbf{k}'|V_3|\mathbf{k}\rangle$ we have

$$k'_{x1} = -\frac{K'_1 + 2K'_3}{\sqrt{2}} = -\frac{k'_{y1} + 2k'_{y3}}{\sqrt{3}} = -\frac{p_{y1} + 2k_{y3}}{\sqrt{3}}, \tag{6.15}$$

which leads to [see (6.10)]

$$k'_{x1} = -\frac{p_{y1} + 2\overline{k_{y3}} + 2\,\eta s_{y3}}{\sqrt{3}}. \tag{6.16}$$

With (6.14) this shows that the intermediate momentum $\mathbf{k}'$ has a fixed value for given initial and final momenta. We have

$$\omega_{k'} = k'^2_{x1} + k'^2_{y1} = \tfrac{4}{3}(p^2_{y1} + p_{y1}k_{y3} + k^2_{y3}). \tag{6.17}$$

Similar to these expressions, let us introduce a momentum $\overline{\mathbf{k}'} = (\overline{k'_{x1}}, \overline{k'_{y1}})$ by [cf. (6.14) and (6.15)]

$$\overline{k'_{x1}} \equiv -\frac{p_{y1} + 2\overline{k_{y3}}}{\sqrt{3}},$$

$$\overline{k'_{y1}} \equiv p_{y1}. \tag{6.18}$$

Then one can write k'_{x1} as

$$k'_{x1} = \overline{k'_{x1}} - \eta' s_{y3}, \tag{6.19}$$

where

$$\eta' \equiv \frac{2}{\sqrt{3}}\,\eta. \tag{6.20}$$

In analogy to (6.10), $\overline{k'_{x1}}$ corresponds to the most probable value of k'_{x1}, which is proportional to the relative momentum of particles 2 and 3 in the intermediate state [see (4.4)]. Similar to (6.17), we have

$$\omega_{\overline{k'}} = (\overline{k'_{x1}})^2 + (\overline{k'_{y1}})^2 = \tfrac{4}{3}(p^2_{y1} + p_{y1}\overline{k_{y3}} + \overline{k^2_{y3}}). \tag{6.21}$$

Then intermediate energy $\omega_{k'}$ can be written as

$$\omega_{k'} = (\overline{k'_{x1}} - \eta' s_{y3})^2 + p^2_{y1} = \omega_{\overline{k'}} - 2\,\eta'\overline{k'_{x1}}s_{y3} + \eta'^2 s^2_{y3}. \tag{6.22}$$

We have condition (4.15). This simplifies the following calculations. If we can impose a similar condition on the intermediate states, the calculations are even more simplified. This is possible, because the value of $\overline{k'_{x1}}$ in the intermediate momentum depends on p_{y1} of the final momentum, as well as k_{y3} in the initial wave packet [see (6.18)]. Hence let us choose the initial and final momenta such that

$$\eta \ll |\overline{k'_{x1}}|. \tag{6.23}$$

Then we can neglect the last term in (6.22), because $|\mathbf{s}|$ is of order 1 [see (6.11)]. We then have

$$\omega_{k'} \approx \omega_{\overline{k'}} - 2\,\eta'\overline{k'_{x1}}s_{y3} = \omega_{\overline{k'}} + 2\,\eta k_{32}s_{y3}, \tag{6.24}$$

where

$$k_{32} \equiv -\frac{2}{\sqrt{3}}\,\overline{k'_{x1}} = \tfrac{2}{3}(p_{y1} + 2\overline{k_{y3}}). \tag{6.25}$$

Here we have introduced the index 32 to emphasize that k_{32} is proportional to the average relative momentum of particles 3 and 2, in the intermediate state [see (4.4)].

With similar approximations, for the energies ω_l and ω'_l [see (6.10)] we obtain

$$\omega_l \approx \omega_{\overline{k}} + 2\,\eta(\overline{\mathbf{k}}\cdot\mathbf{u}), \quad \omega_{l'} \approx \omega_{\overline{k'}} + 2\,\eta k_{32}u_{y3}. \tag{6.26}$$

Equations (6.12), (6.24), and (6.26) show that the deviation of the initial and intermediate energies ω_k, ω_l, $\omega_{k'}$, and $\omega_{l'}$ from their averages is small for a sufficiently large wave packet.

VII. OFF-ON SHELL PROCESS

Now we are ready to evaluate contribution (6.9). We first consider the off-on shell process with the conditions

$$|\omega_p - \omega_{\overline{k'}}| \gg \eta|k_{32}| \quad \text{and} \quad |\omega_p - \omega_{\overline{k'}}| \gg \eta|\overline{\mathbf{k}}|, \tag{7.1}$$

while

$$O(|\omega_{\overline{k'}} - \omega_{\overline{k}}|) = \eta|\overline{\mathbf{k}}| \sim \eta|k_{32}|. \tag{7.2}$$

This is the process corresponding to diagram (d) in Fig. 5. As we shall show, this is a transient process, i.e., this exists only during the collision, and disappears after all interaction processes are finished.

From (6.26) we have

$$w_{pl'} \approx w_{p\overline{k'}} - 2\,\eta k_{32}u_{y3}. \tag{7.3}$$

Equation (7.1) gives us

$$w_{pl'} \approx w_{p\overline{k'}}. \tag{7.4}$$

Similarly we have

$$-w_{k'p}\approx w_{pl}\approx -w_{kp}\approx w_{p\overline{k'}}. \tag{7.5}$$

Then from (6.6) we obtain (for $|z|\sim\epsilon$)

$$\Phi_1(\mathbf{p},\mathbf{k}',\boldsymbol{l}',\mathbf{k},\boldsymbol{l},z)\approx\lambda^4 v_1^2 v_3^2\Delta(\mathbf{p},\mathbf{k}',\boldsymbol{l}',\mathbf{k},\boldsymbol{l})\,\frac{1}{w^2_{p\overline{k'}}}\,\frac{1}{z}\,\frac{1}{z-w_{kl}}\left(\frac{1}{z-w_{k'l}}+\frac{1}{z-w_{kl'}}\right)\left[-\left(1+\frac{z}{z-w_{k'l'}}\right)+1\right]. \tag{7.6}$$

The subscript 1 in Φ_1 denotes that (7.6) is evaluated with conditions (7.1) and (7.2). The first term (with the parentheses) inside the last bracket in (7.6) corresponds to the sum of diagrams (a)–(d) in Fig. 12, while the last term (i.e., 1), to the sum of diagrams (e) and (f). Then we obtain from (6.9) that

$$\langle\langle\mathbf{p};\mathbf{p}|\overline{\rho_1}(t)\rangle\rangle\approx-\lambda^4\,\frac{v_1^2v_3^2}{w^2_{p\overline{k'}}}\int d^2k\;d^2l\int d^2k'd^2l'\Delta(\mathbf{p},\mathbf{k}',\boldsymbol{l}',\mathbf{k},\boldsymbol{l})\,\mathrm{Res}_{\,z=+i\epsilon}\left[\frac{e^{-izt}}{z}\,\frac{1}{z-w_{k'l}}\,\frac{1}{z-w_{kl'}}\left(\frac{z}{z-w_{kl}}+\frac{z}{z-w_{k'l'}}\right)\right]$$
$$\times\langle\langle\mathbf{k};\boldsymbol{l}|\rho(0)\rangle\rangle, \tag{7.7}$$

where 1 in $\overline{\rho_1}$ denotes that this is evaluated for the off-on shell process with Φ_1.

Applying Eqs. (6.12), (6.24), and (6.26), we have

$$w_{k'l'}\approx 2\,\eta k_{23}(s_{y3}-u_{y3}),$$
$$w_{kl}\approx 2\,\eta\overline{\mathbf{k}}\cdot(\mathbf{s}-\mathbf{u})=2\,\eta|\overline{\mathbf{k}}|(s_{\overline{\mathbf{k}}}-u_{\overline{\mathbf{k}}}), \tag{7.8}$$

where $s_{\overline{\mathbf{k}}}\equiv(\mathbf{s}\cdot\overline{\mathbf{k}})/|\overline{\mathbf{k}}|$ is the component of $\mathbf{s}$ in the direction of $\overline{\mathbf{k}}$, and similarly $u_{\overline{\mathbf{k}}}\equiv(\mathbf{u}\cdot\overline{\mathbf{k}})/|\overline{\mathbf{k}}|$. Then the two terms inside the parentheses in (7.7) are written as

$$\frac{i\epsilon}{i\epsilon-2\,\eta k_{23}(s_{y3}-u_{y3})}+\frac{i\epsilon}{i\epsilon-2\,\eta|\overline{\mathbf{k}}|(s_{\overline{\mathbf{k}}}-u_{\overline{\mathbf{k}}})}. \tag{7.9}$$

Similar to two-body scattering, we may define the following two time scales of the duration of the collision [see (3.30)]:

$$t_c=\frac{\sqrt{\pi}}{4\,\eta|\overline{\mathbf{k}}|},\quad t_c'=\frac{\sqrt{\pi}}{4\,\eta|k_{32}|}. \tag{7.10}$$

The processes during and after the collision are distinguished by the limiting procedures of ϵ and η. After the collision we have $t\gg t_c$ and $t\gg t_c'$, which correspond to $\epsilon\ll\eta|\overline{\mathbf{k}}|$ and $\epsilon\ll\eta|k_{32}|$, respectively. In this case (7.9) vanishes, and we have

$$\langle\langle\mathbf{p};\mathbf{p}|\overline{\rho_1}(t)\rangle\rangle\to 0. \tag{7.11}$$

In contrast, during the collision we have $t\ll t_c$ and $t\ll t_c'$, which correspond to $\epsilon\gg\eta|\overline{\mathbf{k}}|$ and $\epsilon\gg\eta|k_{32}|$. For this case we can approximate the initial condition by a plane wave, i.e.,

$$\langle\langle\mathbf{k};\boldsymbol{l}|\rho(0)\rangle\rangle\to\delta(\mathbf{k}-\boldsymbol{l})\,\delta(\mathbf{k}-\overline{\mathbf{k}}). \tag{7.12}$$

We have $\omega_k\approx\omega_l\approx\omega_{\overline{k}}$ and $\omega_{k'}\approx\omega_{l'}\approx\omega_{\overline{k'}}$ [see Eqs. (6.12), (6.24), and (6.26)]. In this case the value of (7.9) becomes 2.

Moreover, the integrations over $\mathbf{k}'$ and $\boldsymbol{l}'$ can be performed using the δ functions. For example, we have [see (F8)]

$$\int dk'_{x_1}\delta(k'_{y_3}-k_{y_3})=\frac{2}{\sqrt{3}}\int dk'_{x_1}\delta\left(k'_{x_1}+\frac{1}{\sqrt{3}}\,k'_{y_1}+\frac{2}{\sqrt{3}}\,k_{y_3}\right). \tag{7.13}$$

This leads to a factor $2/\sqrt{3}$. Similarly we have the same factor by the integration over l'_{x_1}. Then, (7.7) leads to

$$\langle\langle\mathbf{p};\mathbf{p}|\overline{\rho_1}(t)\rangle\rangle\approx-\lambda^4\,\frac{4v_1^2v_3^2}{3w^2_{p\overline{k'}}}\,\mathrm{Res}_{\,z=+i\epsilon}\left[\frac{e^{-izt}}{z^2}\left(\frac{1}{z-w_{\overline{k'}\overline{k}}}+\frac{1}{z+w_{\overline{k'}\overline{k}}}\right)\right]. \tag{7.14}$$

Because of the double pole at $z=+i\epsilon$, this expression gives the asymptotic transition probability as

$$\overline{\rho_1}(\mathbf{p},\mathbf{p},t)\approx 2\pi\lambda^4\,\frac{4v_1^2v_3^2}{3w^2_{\overline{kp}}}\,t\,\delta(\omega_{\overline{k'}}-\omega_{\overline{k}}). \tag{7.15}$$

During the collision, the term we are considering here grows linearly in time, and then vanishes after the collision. This is the transient process.

There are three more processes: the rescattering process, the genuine triple collision process, and the on-off shell process, corresponding to diagrams (a), (b), and (c) in Fig. 5, respectively. We present detailed calculations in Appendices G–I, and here give only the results.

For the genuine triple collision and the on-off shell processes, the transition probabilities grow linearly in time during the collisions, and reach constants after the collisions.

The rescattering process corresponds to two successive two-body collisions. The time interval between the two-body collision may be long. Assuming, for example, that $t_c\ll t_c'$ [see (7.10)], for the rescattering process one may consider three time scales: (1) $t\ll t_c$, (2) $t_c\ll t\ll t_c'$, and (3) $t_c'\ll t$. As shown in Appendix I, the contribution from the rescattering process grows asymptotically as $t^2/2$ in time during time scale (1), and linearly as $t_c't$ during time scale (2), and then reaches a constant proportional to t_ct_c' after all collisions are finished in time scale (3).

As a result of the t^2 secular contribution in the rescattering process, the transition rate per unit time diverges for a

TABLE II. Terms of the transition probability for the (12)–(23) collision process.

	$t \ll t_c', t_c$	$t \gg t_c', t_c$
(a) rescattering	$(2\pi t)^2 \delta(w_{pk'}) \delta(w_{pk})/2$	$(2\pi)^2 t_c t_c' \delta(w_{pk'}) \delta(w_{pk}) \gamma$
(b) triple collision	$(2/w^2_{pk'}) \pi t \delta(w_{kp})$	$(2/w^2_{pk'}) \pi t_c \delta(w_{kp})$
(c) on-off shell	$(2/w^2_{k'k}) \pi t \delta(w_{pk'})$	$(2/w^2_{k'k}) \pi t_c' \delta(w_{pk'})$
(d) off-on shell	$(2/w^2_{kp}) \pi t \delta(w_{k'k})$	~ 0

large time scale during the collision. This corresponds to the well-known *rescattering anomaly* for three-body scattering [6]. This anomaly appears only in the channel between the ''free three particles in'' and ''free three particles out,'' as this is associated to the successive two-body collisions. The origin of this difficulty in the usual S-matrix approach is that the Möller scattering states for the Hamiltonian do not belong to the Hilbert space, as the three-body t matrix in the wave-function space is a distribution in the momentum representation. Hence, when we take the square of the t matrix in evaluating the transition rate, the on-shell processes in the intermediate states lead to the divergence associated to this anomaly. Through the optical theorem of the t matrix, this divergence is related to the divergence of the on-shell three-body t matrix itself.

In contrast, the complex spectral representation for the Liouvillian introduced in our work [9,10] deals consistently with the scattering outside the Hilbert space. After explicitly separating the secular effect of t^2, the true three-body processes associated with t linear secular terms give a finite transition rate for the three-body scattering (this transition rate leads to a finite contribution, even when we integrate it over the domain of the final momentum including the points satisfying the on-on shell condition). Hence our theory removes the difficulty of the rescattering anomaly. The rescattering anomaly itself has been a longstanding problem [19,20]. We shall prove that our theory indeed leads to a divergence-free transition rate for the true three-body scattering in a separate paper [11].

In summary we have obtained the results which are displayed in Table II (abbreviating the common factor $\frac{4}{3}\lambda^4 v_1^2 v_3^2$): Each process (a)–(d) in Table II corresponds to each diagram (a)–(d) in Fig. 5. In (a) the parameter γ is a constant which depends on the direction of the final momentum (see Appendix I). The last process (d) is an effect that can be observed only for finite time during the collision for large wave packets, or for persistent interaction with delocalized density matrices outside Hilbert space.

We note that the difference of the transition probability between the collision and after the collision appears in the secular term proportional to t. This is a striking difference from the two-body scattering discussed in Sec. III. After separating the rescattering contribution, the true three-body scattering cross section is defined by the transition rate per unit time. Our results show that the correction of the true three-body scattering cross section to the one obtained by the S-matrix theory during the collision is of the *same* order as the rest of contributions. In Sec. VIII we shall present some results of numerical simulations to verify our predictions.

VIII. NUMERICAL SIMULATIONS

From the results obtained in Sec. VII, we can predict that the two horizontal lines corresponding to the off-on shell process (d) in Fig. 6 are transient; i.e., they exist only during the collision, and then disappear after the collision. On the other hand, all other lines in Fig. 6 as well as the rescattering peaks remain after the collision (see Table II).

We have verified this prediction by numerical simulations for three-body scattering. We display the numerical results in Figs. 13(a)–13(c) for different times. We have generated them by taking the square of the second-order contribution in the Dyson series obtained by the iteration of the integral equation (3.44), similar to what we did for two-body scattering in Sec. III. In Fig. 13, the results correspond to the initial conditions $k_{x1}=k_{y1}=-1$, $\eta=0.006\,25$, and $\lambda=v_a=1$ for $a=1$, 2, and 3. For these parameters we have $t_c=50.1$ [see (7.10)]. As in the case of two-body scattering, there appear contributions which oscillate rapidly for large time scales as a function of ω_p. They approach zero in the sense of distribution. To compare the numerical simulations to our prediction, we have taken averages of the numerical results over the final momentum with intervals $\Delta\omega=10\eta$, which involve a few periods of these rapid oscillations.

Figure 13(a) is the result at $t=0.1t_c$: the particles have not yet reached an asymptotic state. Figure 13(b) is the result at $t=t_c$, which corresponds to the process *during the collision*. All contributions shown in Fig. 6 can be seen. Figure 13(b) is the result at $t=10t_c$: the particles are in the asymptotic state *after the collision*. This is the final state given by S-matrix theory, shown schematically in Fig. 7. The numerical results confirm our prediction.

IX. DESTRUCTION OF THE FACTORIZABILITY OF DENSITY MATRICES—COLLAPSE OF THE WAVE FUNCTION

In previous sections, for scattering during the collision, we approximated large wave packets by plane waves that lie outside the Hilbert space. In this section we shall more closely investigate this approximation in terms of the evolution of the wave function. We shall show that the density matrix becomes nonfactorizable into a product of wave functions during the collision, for time scales when one can identify the rapid oscillations with distributions making a vanishing contribution. The wave function then collapses due to Poincare's resonance for this time scale.

Let us first consider the two-body scattering discussed in Sec. III. Using the solution of the wave function in (3.42), we can write the density matrix in a factorizable form. Then, for nonforward scattering (3.12) (to second order of λ^2), we have

$$\langle\langle p;p|\rho(t)\rangle\rangle \approx \lambda^2 |\langle p|\Psi_1(t)\rangle|^2 = 4\lambda^2 v_0^2 \int dk \int dl \, \frac{\sin[(\omega_p-\omega_k)t/2]}{\omega_p-\omega_k} \, e^{+i\omega_k t/2} \, \frac{\sin[(\omega_p-\omega_l)t/2]}{\omega_p-\omega_l} \, e^{-i\omega_l t/2} \langle\langle k;l|\rho(0)\rangle\rangle. \tag{9.1}$$

Using (3.23), we have [with $\tau_c' \equiv (\eta\overline{k})^{-1} \sim \tau_c$]

$$\frac{\sin[(\omega_p-\omega_k)t/2]}{\omega_p-\omega_k} \, e^{+i\omega_k t/2} = w_{\overline{kp}}^{-1} \left[1 + \frac{s}{w_{\overline{kp}}\tau_c'} + \frac{s^2}{2w_{\overline{kp}}\tau_c'} \frac{\eta}{\overline{k}} \right]^{-1} \sin\left[\frac{w_{\overline{kp}} t}{2} + s \, \frac{t}{\tau_c'} + s^2 \, \frac{t}{2\tau_c'} \frac{\eta}{\overline{k}} \right]$$
$$\times \exp\left[+ i \left(\frac{\omega_{\overline{k}} t}{2} + s \, \frac{t}{\tau_c'} + s^2 \, \frac{t}{2\tau_c'} \frac{\eta}{\overline{k}} \right) \right]. \tag{9.2}$$

Let us then consider the case during the collision. Assuming t/τ_c' and $(|w_{\overline{kp}}|\tau_c')^{-1}$ are much smaller than unity, we can expand (9.2) in the Taylor series for $s \sim 1$. Then we have [see (3.8)]

$$\frac{\sin[(\omega_p-\omega_k)t/2]}{\omega_p-\omega_k} \, e^{+i\omega_k t/2} = \frac{\sin(w_{p\overline{k}}\overline{t}/2)}{w_{p\overline{k}}} \, e^{+i\omega_{\overline{k}}\overline{t}/2} + O\left(\frac{st}{\tau_c'}\right) + O\left(\frac{s}{|w_{p\overline{k}}|\tau_c'}\right). \tag{9.3}$$

Substituting this and (3.22) into (9.1), we obtain

$$\langle\langle p;p|\rho(t)\rangle\rangle = 4\lambda^2 v_0^2 \left[\frac{\sin(w_{p\overline{k}}\overline{t}/2)}{w_{p\overline{k}}} \right]^2 \frac{1}{2\pi} \left| \int_{-\infty}^{+\infty} ds \; e^{-s^2/2} \right|^2 + O(\lambda^3) + O\left(\frac{\lambda^2 t}{\tau_c'}\right) + O\left(\frac{\lambda^2}{|w_{p\overline{k}}|\tau_c'}\right). \tag{9.4}$$

The value of the integral with the factor $1/2\pi$ in the first term is one [see (3.40)]. Then the first term is precisely the contribution from the plane wave with the momentum k. This verifies the approximation we have used in (3.34).

Moreover, one can verify the following relation under the integration over w with suitable test functions and for $\epsilon \to 0+$ [see Appendix J]

$$4\left[\frac{\sin(wt/2)}{w} \right]^2 = 2\pi\delta(w)t + \left[\frac{1}{(w-i\epsilon)^2} \, (1 - e^{-iwt}) + \text{c.c.} \right]. \tag{9.5}$$

This is valid for all time scales.

Let us then consider the case $t>0$. With a suitable test function $f(w)$ let us consider an oscillating contribution in (9.5), e.g.,

$$I(t) = \int dw \, \frac{f(w)}{(w-i\epsilon)^2} \, e^{-iwt}. \tag{9.6}$$

Since $w = w_{p\overline{k}}$ in (9.4), the integration over w (or over the final momentum p) is bounded from below for a given k. A double pole is located at $w = +i\epsilon$ in the upper-half complex plane of w. Because of the factor $\exp[-iwt]$ we can change the contour of w into the lower-half-plane for $t>0$ without crossing the double pole. This implies that there is no secular contribution associated to the resonance pole at $w = +i\epsilon$ in (9.6). For a large time scale the factor $\exp[-iwt]$ makes a rapidly oscillating contribution as a function of w, and one can neglect this term as compared with the secular term and also with the time-independent terms in (9.5). Similarly the complex conjugate of (9.6) is negligible. Dropping these oscillating terms, we obtain (3.35).

We note that whenever we drop the oscillating terms in (9.5), the density matrix cannot be factorized as a product of wave functions. The secular effect proportional to t in (9.5) corresponds to Poincaré's resonance effect. The separation of the resonance effect from the rapidly oscillating contributions leads to a dynamical mechanism of the collapse of wave functions.

Strictly speaking, the time scale to identify the contribution (9.6) as zero is infinity. In order to achieve the collapse of the wave function in a finite time scale, we need a repetition of the collisions with many scatterers [9]. The effect of the repeated collisions can already be seen in the three-body scattering considered in this paper. Let us demonstrate this for the lowest order contribution in λ of the transition probability for the true three-body nonforward scattering considered in previous sections. We assume the initial wave function is given by a plane wave $|\Psi(0)\rangle = |\overline{\mathbf{k}}\rangle$. Integrating (3.42) twice, we obtain

$$\langle \mathbf{p}|\overline{\Psi}(t)\rangle = \sum_{a\neq b} \Psi^{ab}(t), \tag{9.7}$$

where the bar on Ψ denotes the processes we are looking at, and

$$\Psi^{ab}(t)=\lambda^2 v_a v_b \int_0^t dt_2 \int_0^{t_2} dt_1 e^{-i\omega_p(t-t_2)} e^{-i\omega_{k^{ab}}(t_2-t_1)} e^{-i\omega_{\bar{k}} t_1}$$

$$=-2i\lambda^2 v_a v_b \frac{e^{-i\omega_p t/2}}{w_{k^{ab}\bar{k}}}\left(\frac{\sin[w_{\bar{k}p}t/2]}{w_{\bar{k}p}}\exp[-iw_{\bar{k}p}t/2]-\frac{\sin[w_{k^{ab}p}t/2]}{w_{k^{ab}p}}\exp[-iw_{k^{ab}p}t/2]\right), \tag{9.8}$$

with [see (6.21)]

$$\omega_{k^{ab}}\equiv\tfrac{4}{3}(p_{ya}^2+p_{ya}\bar{k}_{yb}+\bar{k}_{yb}^2). \tag{9.9}$$

Summations a and b in (9.7) are taken over particles 1, 2, and 3. This leads to

$$\langle\langle \mathbf{p};\mathbf{p}|\overline{\rho(t)}\rangle\rangle=\left|\sum_{a\neq b}\langle\mathbf{p}|\Psi_1(t)\rangle\right|^2=\sum_{a\neq b}\sum_{c\neq d}\Psi^{ab}(t)[\Psi^{cd}(t)]^{\text{c.c.}}$$

$$=4\lambda^4\sum_{a\neq b}\sum_{c\neq d}\frac{v_a v_b v_c v_b}{w_{k^{ab}\bar{k}}w_{k^{cd}\bar{k}}}\left\{\left(\frac{\sin(w_{p\bar{k}}\bar{t}/2)}{w_{p\bar{k}}}-\frac{\sin(w_{k^{ab}p}t/2)}{w_{k^{ab}p}}\right)\left(\frac{\sin(w_{p\bar{k}}\bar{t}/2)}{w_{p\bar{k}}}-\frac{\sin(w_{k^{cd}p}t/2)}{w_{k^{cd}p}}\right)\right.$$

$$+2\frac{\sin(w_{p\bar{k}}\bar{t}/2)}{w_{p\bar{k}}}\left[\frac{\sin(w_{k^{ab}p}t/2)}{w_{k^{ab}p}}\sin^2\left(\frac{w_{k^{ab}p}t}{4}\right)+\frac{\sin(w_{k^{cd}p}t/2)}{w_{k^{cd}p}}\sin^2\left(\frac{w_{k^{cd}p}t}{4}\right)\right]$$

$$\left.-2\frac{\sin(w_{k^{ab}p}t/2)\sin(w_{k^{cd}p}t/2)}{w_{k^{ab}p}w_{k^{cd}p}}\sin^2\left(\frac{w_{k^{ab}k^{cd}}t}{4}\right)\right\}. \tag{9.10}$$

As a function of the energy ω_p, this expression oscillates in a much more complicated way than (9.4) for two-body scattering. We present the ω_p dependence of (9.4) for two-body scattering in Fig. 14, as well as that of (9.10) for three-body scattering in Fig. 15 for the same given time $t=10^2$. In the figure we put $\lambda=1$, $v_0=1$, and $v_a=1$ for $a=1$, 2, and 3. In Fig. 14 we plot the case $\omega_{\bar{k}}=2$. In Fig. 15 we plot the case $k_{x1}=k_{y1}=-1$. In order to observe the rescattering effect, we have plotted the ω_p dependence of (9.10) in the same direction of the incident momentum **k**. For three-body scattering there appear several peaks with complex background oscillation. The highest peaks of order 10^9 correspond to the highest secular effect with t^2 that comes from the rescattering terms (i.e., repetition of two-body scattering) for $a=c$ and $b=d$ in (9.10). The peaks of order 10^5–10^7 in the vicinity of the highest peak are small corrections of the rescattering effect. The peaks of order 10^4–10^5 far from the rescattering peak corresponds to the linear secular effect with t that comes from all possible combinations of a, b, c, and d in (9.10). The complex background oscillation leads to nonsecular effects of order 10^3.

The appearance of higher secular effect makes less significant the background oscillation, and one can then neglect this oscillating contribution in the sense of distribution in a shorter time scale than for two-body scattering. Arbitrary higher secular effects of t^n by repetition of the collisions for many-body system in the thermodynamic limit then lead to a finite time scale to approach equilibrium, even when we start with a pure state (e.g., a plane wave) [9]. As the equilibrium state is a mixed state, the wave function collapses in a finite time scale because of the repetition of the collisions for macroscopic systems.

X. CONCLUDING REMARKS

The main result of this paper is the extension of scattering theory for finite time scales during the interaction. For large wave packets we obtain an asymptotic description which is different from the usual S-matrix approach (Table I). We have illustrated our approach for two- and three-body scattering. During the collision there appear effects in scattering cross sections which result from secular effects, but differ from the ones predicted by the S-matrix theory for asymptotic times after the collision. We have verified our predictions by numerical simulations.

The consideration of the process during the interaction is the normal procedure in many-body situations as realized for example in chemical reactions. Let us quote the standard text by Goldberger and Watson [3].

''The analysis of the first and third intervals (i.e., before and after the collision) involves only a kinematic study and can be done in a general and straightforward manner. The description of the interaction of the system (i.e., during the collision) involves the most fundamental and difficult problems in physics.''

Indeed, the description during the collision is closely connected to our work on the extension of quantum theory (or of classical theory as well) beyond the Hilbert space for large Poincaré systems (LPS's). Here LPS's mean nonintegrable systems with continuous spectrum of unperturbed momenta or energy [9,10,21]. This theory applies to persistent scattering using delocalized density matrices (an example is plane waves, discussed in this paper). Persistent interactions require singular distribution functions (i.e. the δ-function singularity in momentum) which lie outside the Hilbert space. The S-matrix theory is no longer valid. We have then obtained complex, irreducible spectral representations of the evolution operators, here the Liouville operator L_H in generalized function space [9,10]. Here ''complex'' means that the eigenvalues of the Liouvillian are complex numbers, whose imaginary part refers to the various irreversible processes, such as decay or diffusion. ''Irreducible'' means that these

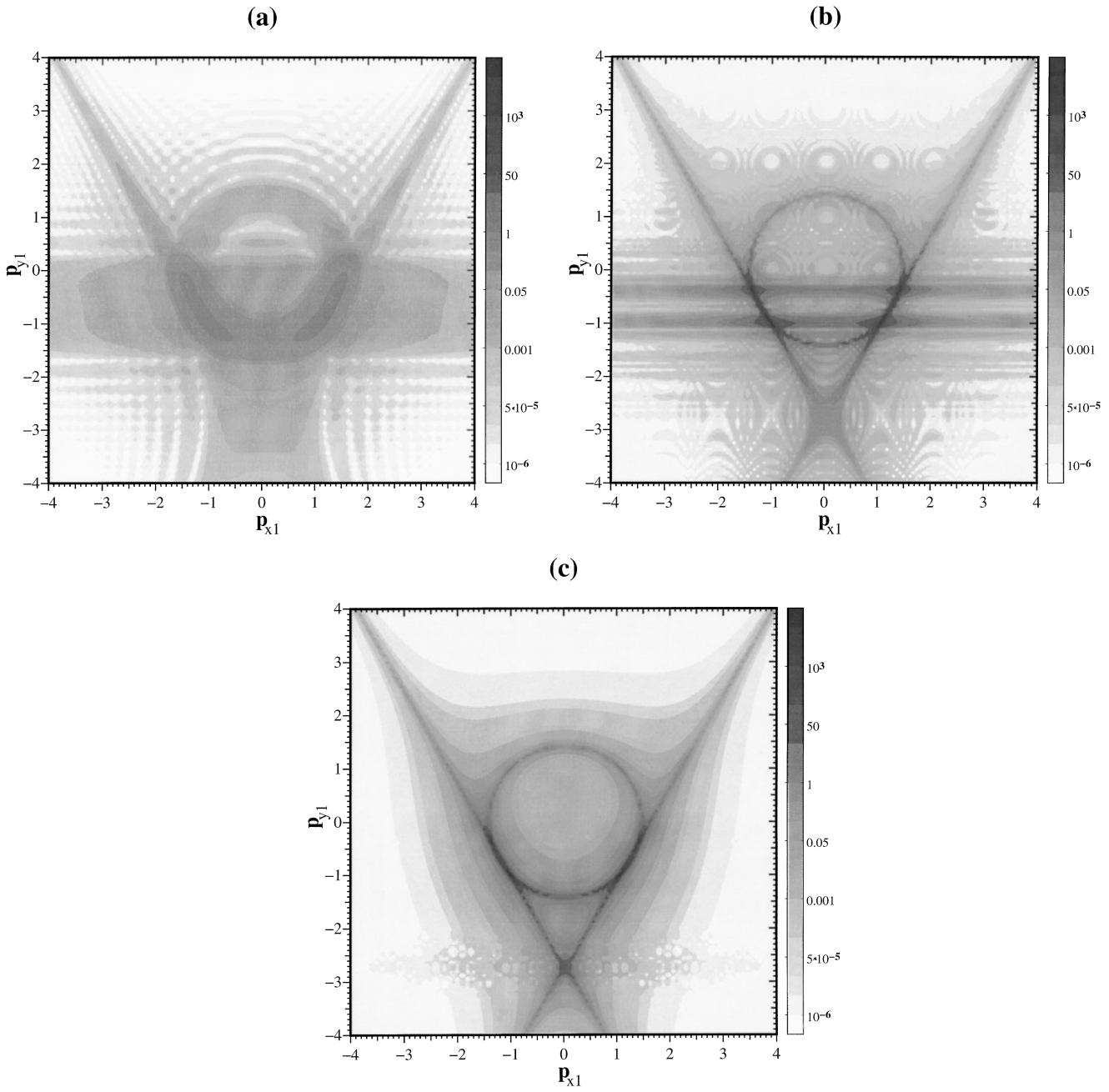

FIG. 13. Numerical results of the final momentum distribution for a succession of a (12) interaction followed by a (23) interaction, in the Jacobi coordinate plane for (a) $t=0.1t_c$, (b) $t=t_c$, and (c) $t=10t_c$ (see text).

representations cannot be implemented by a wave function that is a solution of the Schrödinger equation. As a result, the dynamical group of evolution splits into two semigroups, one oriented to our future, and the other to the past. In the context of scattering theory discussed, irreversibility is manifested as the fact that the scattering cross section is *positive*. As a result of irreducibility, density matrices are no longer factorizable as a product of wave functions for LPS's. This leads to the collapse of wave functions discussed in Sec. IX. Therefore, the equivalence between the *individual* description in terms of wave functions, and the *statistical* description in terms of density matrices, is destroyed. The laws of quantum mechanics take another form as they have to be formulated on the statistical level. They express possibilities and no more certitudes. We shall discuss the relation of the results obtained in this paper and the complex spectral representation elsewhere [21].

In this paper, we have concentrated only on a single process in three-body scattering [i.e., a (12) interaction followed by a (23) interaction]. It is easy to extend our results to other three-body processes. In a subsequent paper, we shall consider all three-body scattering processes and give an explicit expression for the difference in the cross sections obtained by the two asymptotic theories. This may be the starting point for a real world experiment to test the limits of the traditional Hilbert space formulation of quantum theory.

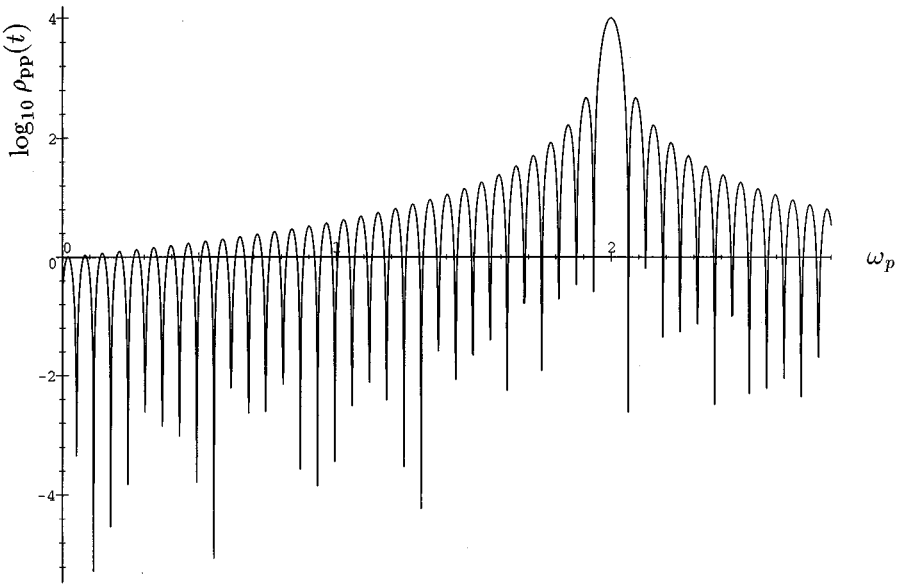

FIG. 14. Transition probability for two-body scattering in logarithmic ($\log_{10}$) scale (see text).

ACKNOWLEDGMENTS

We thank Professor I. Prigogine for his constant interest, encouragement, and helpful suggestions during this work. We also thank Professor Y. Kuperin for fruitful discussions, and H. W. Wong who performed a part of the numerical simulations. We acknowledge the U.S. Department of Energy Grant No. DE-FG03-94ER14465, the Robert A. Welch Foundation Grant No. F-0365, and the European Community Contract No. PSS*0832 for support of this work.

APPENDIX A: *T* MATRICES

Let us introduce the two-body t matrices in wave-function space. They are defined as the solutions of the integral equation (in the Jacobi coordinate system)

$$t^a(z)=\lambda V_a+\lambda V_a\,\frac{1}{z-H_0}\,t^a(z), \tag{A1}$$

where $a=1$, 2, or 3, as usual. For the δ-function interaction considered in this paper, the exact solutions of $t^a(z)$ are given by

$$t^a_{\mathbf{pk}}(z)=\langle\mathbf{p}|t^a(z)|\mathbf{k}\rangle = \lambda v_a\delta(p_{ya}-k_{ya})\left[1+\int d^2l\,\frac{\lambda v_a\delta(l_{ya}-k_{ya})}{\omega_l-z}\right]^{-1}. \tag{A2}$$

Applying the Faddeev expansion with these solutions for the two-body collision, one can construct the three-body t

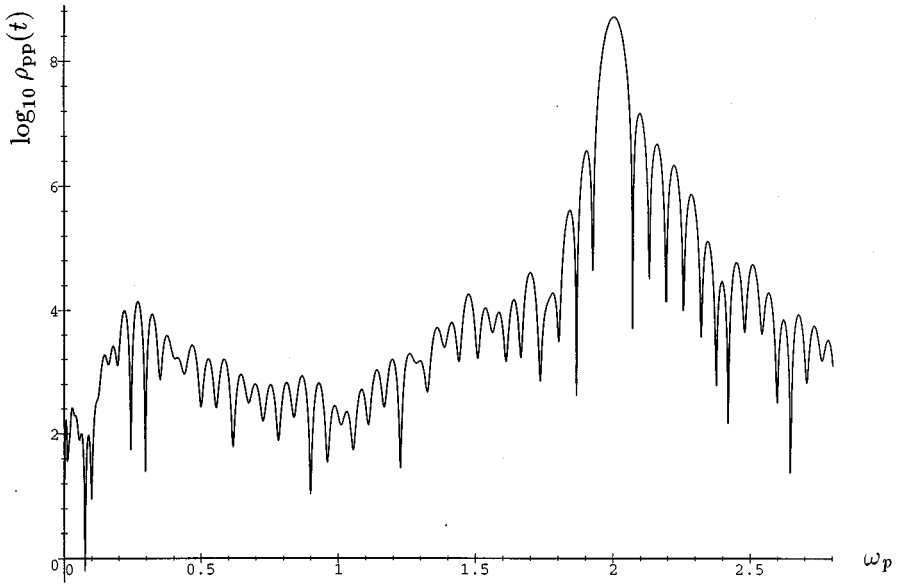

FIG. 15. Transition probability for three-body scattering in logarithmic ($\log_{10}$) scale (see text).

matrix. The characteristic of the Faddeev expansion is that in each term in the expansion there is no successive repetition of the two-body t matrices with the same index a for the process involving all three particles. This rearrangement of the series expansion leads to a well-defined three-body t matrix in wave-function space [18].

Corresponding to the two-body t matrices in wave-function space, we can introduce $T_a^>(z)$ and $T_a^<(z)$ in Liouville space. They satisfy, respectively,

$$T_a^>(z)=(\lambda V_a\times 1)+(\lambda V_a\times 1)\,\frac{1}{z-L_0}\,T_a^>(z), \quad \text{(A3)}$$

$$-T_a^<(z)=-(1\times\lambda V_a)-(1\times\lambda V_a)\,\frac{1}{z-L_0}\,[-T_a^<(z)]. \quad \text{(A4)}$$

They are related to t_a by

$$\langle\langle \mathbf{p};\mathbf{p}'|T_a^>(z)|\mathbf{k};\mathbf{k}'\rangle\rangle = t^a_{\mathbf{pk}}(z+\omega_{k'})\,\delta(\mathbf{k}'-\mathbf{p}'), \quad \text{(A5)}$$

$$\langle\langle \mathbf{p};\mathbf{p}'|T_a^<(z)|\mathbf{k};\mathbf{k}'\rangle\rangle = \delta(\mathbf{p}-\mathbf{k})t^a_{\mathbf{k}'\mathbf{p}'}(-z+\omega_k). \quad \text{(A6)}$$

Replacing $V_a\times 1$ and $1\times V_a$, the diagrams in Fig. 12, by $T_a^>$ and $T_a^<$, respectively, we obtain the simplest true three-body nonforward scattering in all order of λ. For example, corresponding to (6.4), we have

$$\frac{1}{z-w_{pp}}\,t^1_{\mathbf{pk}'}(z+\omega_p)\,\frac{1}{z-w_{k'p}}\,t^3_{\mathbf{k}'\mathbf{k}}(z+\omega_p) \times\frac{1}{z-w_{kp}}\,[-t^1_{\mathbf{l}'\mathbf{p}}(-z+\omega_k)]\,\frac{1}{z-w_{kl'}}\,[-t^3_{\mathbf{ll}'}(-z+\omega_k)] \times\frac{1}{z-w_{kl}}. \quad \text{(A7)}$$

Performing a similar replacement in the results obtained in the text, we obtain the exact form of the transition probability of true three-body nonforward scattering that involves the rescattering process.

APPENDIX B: EVALUATION OF INTEGRATION (3.25)

In this appendix we shall prove that

$$I(\beta,\mu)\equiv\int_{-\infty}^{\infty}ds\,\frac{1}{s+\beta}\,e^{-\mu^2s^2} =-\pi i e^{-\mu^2\beta^2}\left[\operatorname{sgn}(\operatorname{Im}\beta)+\frac{2i}{\sqrt{\pi}}\operatorname{erfi}(\mu\beta)\right], \quad \text{(B1)}$$

which holds for

$$\operatorname{Im}\beta\neq 0 \quad |\arg(\mu)|<\pi/4. \quad \text{(B2)}$$

Here, $\operatorname{erfi}(x)$ is the imaginary error function defined by

$$\operatorname{erfi}(x)\equiv -i\,\operatorname{erf}(ix), \quad \operatorname{erf}(x)\equiv\int_0^x e^{-t^2}dt. \quad \text{(B3)}$$

For

$$\beta=\frac{1}{2\eta k}(w_{\overline{kp}}-i\epsilon), \quad \mu=\frac{1}{\sqrt{2}}, \quad \text{(B4)}$$

we have the integration in (3.25), i.e.,

$$\left|\int_{-\infty}^{\infty}ds\;e^{-(1/2)s^2}\,\frac{1}{-i\epsilon+w_{\overline{kp}}+2\eta\overline{ks}}\right|^2=\left(\frac{1}{2\eta k}\right)^2|I(\beta,\mu)|^2, \quad \text{(B5)}$$

that leads to (3.26).

Let us start with a well-known integral [22]

$$I_0(\gamma,\mu)\equiv\int_{-\infty}^{\infty}ds\,\frac{1}{s^2+\gamma^2}\,e^{-\mu^2s^2} =\frac{\pi e^{\mu^2\gamma^2}}{\gamma}\left[1-\frac{2}{\sqrt{\pi}}\operatorname{erf}(\mu\gamma)\right], \quad \text{(B6)}$$

which holds for $\operatorname{Re}\gamma>0$ and $|\arg(\mu)|<\pi/4$. As $I_0(\gamma,\mu)=I_0(-\gamma,\mu)$, we can extend this formula for $\operatorname{Re}\gamma\neq 0$, by replacing the 1 inside the brackets by $\operatorname{sgn}(\operatorname{Re}\gamma)$.

Putting $\gamma\equiv i\beta$, we have $\operatorname{Re}\gamma\neq 0$ for (B4) (recall that $\epsilon>0$). Hence we can apply (B6) to the integral

$$I_1(\beta,\mu)\equiv\int_{-\infty}^{\infty}ds\,\frac{1}{s^2-\beta^2}\,e^{-\mu^2s^2}=I_0(i\beta,\mu) =-\frac{\pi e^{-\mu^2\beta^2}}{i\beta}\left[\operatorname{sgn}(\operatorname{Im}\beta)+\frac{2i}{\sqrt{\pi}}\operatorname{erfi}(\mu\beta)\right]. \quad \text{(B7)}$$

On the other hand, we have

$$I(\beta,\mu)-I(-\beta,\mu)=-2\beta I_1(\beta,\mu), \quad \text{(B8)}$$

as well as

$$I(\beta,\mu)=\tfrac{1}{2}[I(\beta,\mu)-I(-\beta,\mu)]. \quad \text{(B9)}$$

Combining these results, we obtain the desired result (B1).

Using the asymptotic expansions of the error function (erfi) for small and large arguments, we obtain the following approximations for $\operatorname{Im}\beta<0$.

For $|\beta|\ll 1$,

$$I\left(\beta,\frac{1}{\sqrt{2}}\right)\simeq\pi i e^{-\beta^2/2}, \quad \text{(B10)}$$

and, for $|\beta|\gg 1$,

$$I\left(\beta,\frac{1}{\sqrt{2}}\right)\simeq\frac{\sqrt{2\pi}}{\beta}. \quad \text{(B11)}$$

APPENDIX C: ON SHELL TWO-BODY TRANSITION PROBABILITY

In this appendix we shall prove (3.29). We shall start with (3.25), i.e.,

$$\langle\langle p;p|\rho(t)\rangle\rangle \approx \lambda^2 v_0^2 \int_{-\infty}^{\infty} ds \int_{-\infty}^{\infty} du \; \frac{1}{-i\epsilon - w_{\bar{k}p} + 2\eta\bar{k}u} \; \frac{1}{i\epsilon - w_{\bar{k}p} - 2\eta\bar{k}s} \; \frac{1}{2\pi} \; e^{-(1/2)(s^2+u^2)}. \tag{C1}$$

We are interested in the integration of this expression over a set of final states $\omega_{\bar{k}} - \Delta\omega \leqslant \omega_p \leqslant \omega_{\bar{k}} + \Delta\omega$, that includes the resonance peak at $\omega_p = \omega_{\bar{k}}$ [with a suitable test function $f(\omega_p)$]

$$I \equiv \int_{\omega_{\bar{k}} - \Delta\omega}^{\omega_{\bar{k}} + \Delta\omega} d\omega_p f(\omega_p) \langle\langle p;p|\rho(t)\rangle\rangle = I_1 + I_2 + I_3, \tag{C2}$$

where

$$I_1 \equiv \int_{-\infty}^{+\infty} d\omega_p f(\omega_p) \langle\langle p;p|\rho(t)\rangle\rangle \tag{C3}$$

and

$$I_2 \equiv -\int_{\omega_{\bar{k}} + \Delta\omega}^{+\infty} d\omega_p f(\omega_p) \langle\langle p;p|\rho(t)\rangle\rangle,$$

$$I_3 \equiv -\int_{-\infty}^{\omega_{\bar{k}} - \Delta\omega} d\omega_p f(\omega_p) \langle\langle p;p|\rho(t)\rangle\rangle. \tag{C4}$$

We assume that the test function $f(\omega_p)$ is bounded from above in the vicinity of the real axis of ω_p, i.e., $|f(\omega_p)| < M$, and does not vanish at the resonance point $\omega_p = \omega_{\bar{k}}$, and that it varies smoothly enough around the resonance peak for small enough η. Moreover, we assume that the domain of the integration is taken as

$$\frac{|f(\omega_{\bar{k}})|}{M} \gg \frac{\eta|\bar{k}|}{\Delta\omega}. \tag{C5}$$

We note that residues at zeros of the denominator in the integration over ω_p in (C2) are of order $(\eta k)^{-1}$, which make large contributions for small η. Hence we also assume that any contributions from the singularities of $f(\omega_p)$ in the complex plane are negligible in the integration (C2) as compared with these residues for small enough η.

Under these conditions we shall show that I_1 makes the dominant contribution to I. Closing the contour of integration in the upper infinite semicircle in I_1, we obtain

$$I_1 \approx 2\pi i \lambda^2 v_0^2 \int_{-\infty}^{\infty} ds \int_{-\infty}^{\infty} du \; \frac{1}{2\eta\bar{k}(u-s) + i\epsilon} \; \frac{1}{2\pi} \times e^{-(1/2)(s^2+u^2)} f(\omega_{\bar{k}} + 2\eta\bar{k}u). \tag{C6}$$

Because of (3.8), we have $\omega_{\bar{k}} \gg \eta|\bar{k}|$. Then we approximate $f(\omega_{\bar{k}} + 2\eta\bar{k}u) \approx f(\omega_{\bar{k}})$ in (C6). One can evaluate the integral by changing the variable $v \equiv u - s$ and using formula (B10). The result is

$$\int_{-\infty}^{\infty} ds \int_{-\infty}^{\infty} du \; \frac{1}{a(u-s) + i\epsilon} \; e^{-(1/2)(s^2+u^2)} = -\frac{1}{|a|} \; i\pi^{3/2}. \tag{C7}$$

Hence we obtain [with $\tau_c \equiv \sqrt{\pi}/(4\eta|\bar{k}|)$]

$$I_1 = \lambda^2 v_0^2 \pi^{3/2} \frac{1}{2\eta|\bar{k}|} f(\omega_{\bar{k}}) = 2\pi\lambda^2 v_0^2 \tau_c f(\omega_{\bar{k}}). \tag{C8}$$

For I_2, the denominator of the integrand is outside the resonance peak at $w_{p\bar{k}} = 0$. Then we have

$$|I_2| \leqslant \int_{\omega_{\bar{k}} + \Delta\omega}^{+\infty} d\omega_p \; \frac{|f(\omega_p)|}{w_{p\bar{k}}^2} \leqslant \lambda^2 v_0^2 \; \frac{M}{\Delta\omega}. \tag{C9}$$

Hence we have

$$\left|\frac{I_2}{I_1}\right| \leqslant \frac{M}{|f(\omega_{\bar{k}})|} \; \frac{2\eta\bar{k}}{\pi^{3/2}\Delta\omega} \ll 1. \tag{C10}$$

Similarly we have

$$\left|\frac{I_3}{I_1}\right| \ll 1. \tag{C11}$$

Therefore, the dominant contribution of the transition probability comes around the resonance peak, and we obtain

$$\langle\langle p;p|\rho(t)\rangle\rangle \approx 2\pi\lambda^2 v_0^2 \tau_c \delta(\omega_p - \omega_{\bar{k}}),$$

which is the desired result (3.31).

APPENDIX D: DURATION OF COLLISION τ_c

The exact value of the duration of collision is not obvious for the Gaussian wave packet. Instead we can consider a wave packet with rectangular shape of size $\sqrt{\pi}/\eta$ defined in configuration space,

$$\langle x|\Psi(0)\rangle = \left[\theta\left(x + \frac{\sqrt{\pi}}{2\eta}\right) - \theta\left(x - \frac{\sqrt{\pi}}{2\eta}\right)\right] \frac{1}{\sqrt{2\pi}} \; e^{-i\bar{k}x}, \tag{D1}$$

where $\theta(x)$ is a step function, $\theta(x) = 0$, for $x < 0$, while $\theta(x) = 1$, for $x \geqslant 0$. We have

$$\langle k|\Psi(0)\rangle = \frac{\sin[\sqrt{\pi}(k-\bar{k})/2\eta]}{\pi(k-\bar{k})} \to \delta(k-\bar{k}) \quad \text{for} \quad \eta \to 0. \tag{D2}$$

Moreover, we have [see (3.7)]

$$\langle\Psi(0)|\Psi(0)\rangle = \frac{\sqrt{\pi}}{\eta}. \tag{D3}$$

Because the interaction starts in the middle of the wave packet at $x = 0$, and moves with a momentum around k with a mass $m = \frac{1}{2}$ [see (3.1)], the duration of collision τ_c is given by

$$\tau_c=\frac{\sqrt{\pi}}{2\eta}\frac{1}{2|\overline{k}|}=\frac{\sqrt{\pi}}{4\eta|\overline{k}|}. \tag{D4}$$

This is the same as (3.30).

APPENDIX E: ON ϵ

In the limit $L\to\infty$, the propagators become the distribution (for $\epsilon\to 0+$)

$$\frac{1}{w_\nu\pm i\epsilon}\to\mathscr{P}\frac{1}{w_\nu}\mp i\pi\delta(w_\nu), \tag{E1}$$

where $\mathscr{P}$ stands for the principal part. The use of the δ function $\delta(w_\nu)$ is possible only because we consider the momentum k as a continuous variable. For finite ϵ the δ function $\pi\delta(w_\nu)$ is approximated by the Lorentzian distribution $\epsilon/(w_\nu^2+\epsilon^2)$. To obtain a consistent evaluation for the δ function in terms of the box normalization formalism, there should be enough discrete states around the peak of the Lorentzian. Therefore, our expressions have to be understood in the continuous limit $\Delta k\equiv 2\pi/L\to 0$ and $\epsilon\to 0+$, with the condition

$$\frac{|dw_\nu/dk|\Delta k}{\epsilon}\to 0. \tag{E2}$$

In the text, we always consider the limit in this sense.

APPENDIX F: ON THE JACOBI COORDINATES

Generating function

For the Jacobi momenta

$$k_{ya}=\sqrt{\tfrac{3}{2}}K_a,$$

$$k_{xa}=\frac{K_b-K_c}{\sqrt{2}}, \tag{F1}$$

$$K=K_a+K_b+K_c,$$

the generating function is

$$F=\sqrt{\tfrac{2}{3}}k_{ya}R_a+\tfrac{1}{2}(\sqrt{2}k_{xa}+K-\sqrt{\tfrac{2}{3}}k_{ya})R_b + \tfrac{1}{2}(-\sqrt{2}k_{xa}+K-\sqrt{\tfrac{2}{3}}k_{ya})R_c, \tag{F2}$$

where (a,b,c) is a cyclic permutation of (1,2,3). The canonical conjugates of the Jacobi momenta are r_{xa}, r_{ya}, and r_a. They are given by

$$r_a=\frac{\partial F}{\partial K}=\tfrac{1}{2}(R_b+R_c),$$

$$r_{ya}=\frac{\partial F}{\partial k_{ya}}=\sqrt{\tfrac{2}{3}}(R_a-r_a), \tag{F3}$$

$$r_{xa}=\frac{\partial F}{\partial k_{xa}}=\frac{1}{\sqrt{2}}(R_b-R_c).$$

The unperturbed Hamiltonian can be written as

$$H_0\equiv K_a^2+K_b^2+K_c^2=k_{xa}^2+k_{ya}^2+\tfrac{1}{2}K^2-\sqrt{\tfrac{2}{3}}Kk_{ya}. \tag{F4}$$

The equations of motion lead to (for $R\equiv R_a+R_b+R_c$)

$$\frac{dR}{dt}=2K. \tag{F5}$$

In the center-of-mass system we have $K=0$. Then R is a constant of motion. We choose $R=0$. Moreover, (F4) gives us

$$H_0=k_{xa}^2+k_{ya}^2. \tag{F6}$$

Relation among Jacobi's coordinates

Writing (F2) for the (a,b,c) and (b,c,a) permutations we find, for $K=0$,

$$K_a=\frac{\partial F}{\partial R_a}=\sqrt{\tfrac{2}{3}}k_{ya}=-\frac{k_{xb}}{\sqrt{2}}-\frac{k_{yb}}{\sqrt{6}},$$

$$K_b=\frac{\partial F}{\partial R_b}=\sqrt{\tfrac{2}{3}}k_{yb}=\frac{k_{xa}}{\sqrt{2}}-\frac{k_{ya}}{\sqrt{6}}. \tag{F7}$$

Hence

$$k_{ya}=-\frac{\sqrt{3}}{2}k_{xb}-\tfrac{1}{2}k_{yb},$$

$$k_{xa}=\frac{1}{\sqrt{3}}k_{ya}+\frac{2}{\sqrt{3}}k_{yb}=-\tfrac{1}{2}k_{xb}+\frac{\sqrt{3}}{2}k_{yb}, \tag{F8}$$

or

$$\begin{pmatrix}k_{xa}\\k_{ya}\end{pmatrix}=\begin{pmatrix}\cos(2\pi/3) & \sin(2\pi/3)\\ -\sin(2\pi/3) & \cos(2\pi/3)\end{pmatrix}\begin{pmatrix}k_{xb}\\k_{yb}\end{pmatrix}. \tag{F9}$$

Similarly, transformations for (r_{xa},r_{ya}) are given by the same expression as (F9), but with the replacement of $\mathbf{k}$ by $\mathbf{r}$ [see (4.6)].

APPENDIX G: ON-OFF SHELL PROCESS

In this appendix we shall evaluate the on-off shell process which corresponds to process (c) in Fig. 6, as well as in Table II. We consider a process with the conditions

$$O(|\omega_p-\omega_{\overline{k'}}|)=\eta|\overline{\mathbf{k}}|\sim\eta|k_{32}|, \tag{G1}$$

while

$$|\omega_{\overline{k'}}-\omega_{\overline{k}}|\gg\eta|k_{32}| \quad\text{and}\quad |\omega_{\overline{k'}}-\omega_{\overline{k}}|\gg\eta|\overline{\mathbf{k}}|. \tag{G2}$$

From (6.24) and (6.26), we have

$$w_{k'l}=\omega_{k'}-\omega_l\approx w_{\overline{k'}\,\overline{k}}+2\eta(k_{32}s_{y3}-\overline{\mathbf{k}}\cdot\mathbf{u}). \tag{G3}$$

Hence, (for $|\mathbf{s}|\sim|\mathbf{u}|\sim 1$) we have

$$w_{k'l}\approx w_{\overline{k'}\,\overline{k}}. \tag{G4}$$

By the same condition (G2) we also have

$$-w_{kl'}\approx w_{pl}\approx -w_{kp}\approx w_{\overline{k'}\,\overline{k}}. \tag{G5}$$

Substituting these approximations into (6.6), we obtain (for $|z|\sim\epsilon$)

$$\Phi_2(\mathbf{p},\mathbf{k}',\boldsymbol{l}',\mathbf{k},\boldsymbol{l},z)\approx\lambda^4\,\frac{v_1^2v_3^2}{w^2_{\overline{k'}\,\overline{k}}}\,\Delta(\mathbf{p},\mathbf{k}',\boldsymbol{l}',\mathbf{k},\boldsymbol{l})\,\frac{1}{z}\left(\frac{1}{z-w_{pl'}}+\frac{1}{z-w_{k'p}}\right)\left[-\left(\frac{1}{z-w_{kl}}+\frac{1}{z-w_{k'l'}}\right)+\frac{1}{z-w_{kl}}\right], \tag{G6}$$

where we have considered the case $|w_{\overline{k'}\,\overline{k}}|\gg\epsilon$ [see (G2)], and used the relations

$$\frac{1}{z-a}\,\frac{1}{z-b}=\left(\frac{1}{z-a}+\frac{1}{z-b}\right)\,\frac{1}{2z-a-b}, \tag{G7}$$

and also

$$w_{k'l}+w_{kl'}=w_{kl}+w_{k'l'}\,. \tag{G8}$$

The subscript 2 in Φ_2 denotes that (G6) is evaluated for the on-off shell process with the conditions (G1) and (G2).

The first term (with the parentheses) inside the last bracket in (G6) corresponds to the sum of diagrams (a)–(d) in Fig. 12, while the last term corresponds to the sum of diagrams (e) and (f). A part of the contribution of diagrams (a)–(d) cancels with the contribution of (e) and (f). Then from (6.9) we have

$$\langle\langle\mathbf{p};\mathbf{p}|\overline{\rho_2}(t)\rangle\rangle\approx-\lambda^4\,\frac{v_1^2v_3^2}{w^2_{\overline{k'}\,\overline{k}}}\int d^2k\;d^2l\int d^2k'd^2l'\Delta(\mathbf{p},\mathbf{k}',\boldsymbol{l}',\mathbf{k},\boldsymbol{l})\,\mathrm{Res}_{\,z=+i\epsilon}\left[\frac{e^{-izt}}{z}\left(\frac{1}{z-w_{pl'}}+\frac{1}{z-w_{k'p}}\right)\,\frac{1}{z-w_{k'l'}}\right]$$
$$\times\langle\langle\mathbf{k};\boldsymbol{l}|\rho(0)\rangle\rangle, \tag{G9}$$

where 2 in $\overline{\rho_2}$ donotes that this is evaluated for the on-off shell process with Φ_2.

The integrations over $\mathbf{k}'$ and $\boldsymbol{l}'$ can be performed using the δ functions [see (7.13)]. Moreover, using the variables $\mathbf{s}$ and $\mathbf{u}$ in (6.10), and also using Eqs. (6.24) and (6.26), we obtain

$$\langle\langle\mathbf{p};\mathbf{p}|\overline{\rho_2}(t)\rangle\rangle\approx-\lambda^4\,\frac{4v_1^2v_3^2}{3w^2_{\overline{k'}\,\overline{k}}}\left[\int_{-\infty}^{\infty}ds_{x3}\int_{-\infty}^{\infty}du_{x3}\,\frac{1}{2\pi}\,e^{-(1/2)(s_{x3}^2+u_{x3}^2)}\right]\mathrm{Res}_{\,z=+ie}\left[\frac{e^{-izt}}{z}\int_{-\infty}^{\infty}ds_{y3}\int_{-\infty}^{\infty}du_{y3}\,\frac{1}{2\pi}\,e^{-(1/2)(s_{y3}^2+u_{y3}^2)}\right.$$
$$\left.\times\left(\frac{1}{z-w_{p\overline{k'}}-2\eta k_{32}u_{y3}}-\frac{1}{-z-w_{p\overline{k'}}-2\eta k_{32}s_{y3}}\right)\,\frac{1}{z-2\eta k_{32}(s_{y3}-u_{y3})}\right]. \tag{G10}$$

The integrations over s_{x3} and u_{x3} inside the first bracket give 1. Then with a simple manipulation we obtain [see (3.24)]

$$\langle\langle\mathbf{p};\mathbf{p}|\overline{\rho_2}(t)\rangle\rangle\approx\lambda^4\,\frac{4v_1^2v_3^2}{3w^2_{\overline{k'}\,\overline{k}}}\,\mathrm{Res}_{\,z=+i\epsilon}\left[\frac{e^{-izt}}{z}\int_{-\infty}^{\infty}ds_{y3}\int_{-\infty}^{\infty}du_{y3}\,\frac{1}{2\pi}\,e^{-(1/2)(s_{y3}^2+u_{y3}^2)}\,\frac{1}{z-w_{p\overline{k'}}-2\eta k_{32}u_{y3}}\right.$$
$$\left.\times\frac{1}{-z-w_{p\overline{k'}}+2\eta k_{32}s_{y3}}\left(1+\frac{z}{z-2\eta k_{32}(s_{y3}-u_{y3})}\right)\right]. \tag{G11}$$

Let us first consider the case after the collision. The usual scattering theory deals with this situation. For this case we can drop the second term inside the bracket (we have $\eta|k_{32}|\gg\epsilon$). In this time scale, all interaction processes have already finished. Hence the transition probability should reach a constant value. Indeed, (G11) contains only the first-order pole at $z=+i\epsilon$, and its residue gives us a constant (for $t\gg t_c'$)

$$\overline{\rho_2}(\mathbf{p},\mathbf{p},t)\approx\lambda^4\,\frac{4v_1^2v_3^2}{3w^2_{\overline{k'}\,\overline{k}}}\,\frac{1}{2\pi}\left|\int_{-\infty}^{\infty}ds\;e^{-(1/2)s^2}\,\frac{1}{i\epsilon-w_{p\overline{k'}}-2\eta k_{32}s}\right|^2. \tag{G12}$$

Similar to (3.25), we obtain [see (B5)]

$$\langle\langle\mathbf{p};\mathbf{p}|\overline{\rho_2}(t)\rangle\rangle\approx\lambda^4\,\frac{4v_1^2v_3^2}{3w^2_{\overline{k'}\,\overline{k}}}\,\frac{2}{\pi}\,\frac{1}{2\eta k_{32}}\,e^{-w^2_{p\overline{k'}}/(2\eta k_{32})^2}\left|\mathrm{sgn}(k_{32})-\frac{2i}{\sqrt{\pi}}\,\mathrm{erfi}\left(\frac{w_{p\overline{k'}}}{2\sqrt{2}\,\eta k_{32}}\right)\right|^2. \tag{G13}$$

The condition of the on-shell transition between the intermediate and the final states is given by

$$O(|w_{p\overline{k'}}|)=\eta|k_{32}|. \tag{G14}$$

With this condition, we obtain from (G12) that [see (3.31)]

$$\langle\langle \mathbf{p};\mathbf{p}|\overline{\rho_2}(t)\rangle\rangle \approx 2\pi\lambda^4\,\frac{4v_1^2v_3^2}{3(\omega_{\overline{k'}}-\omega_{\overline{k}})^2}\,t_c'\,\delta(\omega_p-\omega_{\overline{k'}}), \tag{G15}$$

where t_c' is given in (7.10).

Next let us consider the case during the collision ($t\ll t_c'$). For this case we can approximate the initial wave packet by a plane wave with $\eta\to 0$, as mentioned in (3.16). Then from (G11) we obtain

$$\begin{aligned}\langle\langle \mathbf{p};\mathbf{p}|\overline{\rho_2}(t)\rangle\rangle &\approx 2\lambda^4\,\frac{4v_1^2v_3^2}{3w^2_{\overline{k'k}}}\,\mathrm{Res}_{\,z=+i\epsilon}\left[\frac{e^{-izt}}{z}\,\frac{1}{z-w_{p\overline{k'}}}\,\frac{1}{-z-w_{p\overline{k'}}}\right]\frac{1}{2\pi}\left[\int_{-\infty}^{\infty}ds\;e^{-(1/2)s^2}\right]^2\\ &=\lambda^4\,\frac{4v_1^2v_3^2}{3w^2_{\overline{k'k}}}\,\mathrm{Res}_{\,z=+i\epsilon}\left[\frac{e^{-izt}}{z^2}\left(\frac{1}{w_{p\overline{k'}}-z}-\frac{1}{w_{p\overline{k'}}+z}\right)\right],\end{aligned} \tag{G16}$$

where we have performed the integration over s.

In contrast to the case after the collision, the transition probability during the collision should change in time, as the interaction processes are not yet finished. Indeed, (G16) now contains the second-order pole at $z=+i\epsilon$, and its residue gives us a linear dependence in time (for $t\ll t_c'$),

$$\langle\langle \mathbf{p};\mathbf{p}|\overline{\rho_2}(t)\rangle\rangle \approx 2\pi\lambda^4\,\frac{4v_1^2v_3^2}{3(\omega_{\overline{k'}}-\omega_{\overline{k}})^2}\,t\,\delta(\omega_p-\omega_{\overline{k'}}), \tag{G17}$$

where we have used relation (3.36). The contribution in (G17) comes from the energies which satisfy the resonance condition $\omega_p-\omega_{\overline{k'}}=0$

Comparing (G17) with (G15), we see the continuation of the transition probability for the on-off shell process during and after the collision. During the collision, it grows linearly in time, and after the collision it becomes a constant.

It is worthwhile to note that the transition probability (G12) after the collision is given by a square of the transition amplitude, just the same as (3.27), i.e. (for $t\to+\infty$),

$$\langle\langle \mathbf{p};\mathbf{p}|\rho(t)\rangle\rangle\to|\langle\mathbf{p}|\Omega_H(\omega_p+i\epsilon)|\Psi(0)\rangle|^2. \tag{G18}$$

Applying this to the fourth-order contribution corresponding to the process which we are considering, we have

$$\begin{aligned}\langle\langle \mathbf{p};\mathbf{p}|\overline{\rho_2}(t)\rangle\rangle = \Big|\lambda^2 v_1 v_3\int d^2k\int d^2k'\,\delta(k'_{y_1}-p_{y_1})\\ \times\delta(k'_{y_3}-k_{y_3})\,\frac{1}{i\epsilon-w_{k'p}}\,\frac{1}{i\epsilon-w_{kp}}\\ \times\langle\mathbf{k}|\Psi(0)\rangle\Big|^2.\end{aligned} \tag{G19}$$

With conditions (G1) and (G2) one can easily show that (G19) reduces to the same expression (G12). However, this derivation with the S-matrix theory is applicable only for the case after the collision. Indeed, if we apply (3.16) to (G19), we obtain a diverging contribution of order ϵ^{-1}, as one can easily verify by a straightforward calculation. In contrast, our complex spectral representation leads to a consistent result with the time-dependent analysis for the process during the collision for a large wave packet [21].

APPENDIX H: GENUINE TRIPLE COLLISION

For the triple collision, we have

$$O(|w_{\overline{kp}}|)=\eta|\overline{\mathbf{k}}|\sim\eta|k_{32}|, \tag{H1}$$

while

$$|w_{\overline{k'k}}|\gg\eta|\overline{\mathbf{k}}|,\quad |w_{\overline{k'k}}|\gg\eta|k_{32}|. \tag{H2}$$

We have

$$w_{k'l}\approx w_{\overline{k'k}}+2\eta(k_{32}s_{y_3}-\overline{\mathbf{k}}\cdot\mathbf{u})\approx w_{\overline{k'k}}. \tag{H3}$$

Similarly,

$$-w_{kl'}\approx -w_{pl'}\approx w_{k'p}\approx w_{\overline{k'k}}. \tag{H4}$$

Hence the first term inside the brackets in (6.6) is negligible, as (for $|z|\sim\epsilon$)

$$\frac{1}{z-w_{pl'}}+\frac{1}{z-w_{k'p}}\approx\frac{1}{-w_{pl'}}+\frac{1}{-w_{k'p}}\approx 0. \tag{H5}$$

Then from its second term, we have

$$\begin{aligned}\Phi_3(\mathbf{p},\mathbf{k}',\boldsymbol{l}',\mathbf{k},\boldsymbol{l},z)\approx-\lambda^4v_1^2v_3^2\Delta(\mathbf{p},\mathbf{k}',\boldsymbol{l}',\mathbf{k},\boldsymbol{l})\,\frac{1}{w^2_{\overline{kk'}}}\\ \times\left(\frac{1}{z-w_{pl}}+\frac{1}{z-w_{kp}}\right)\frac{1}{z-w_{kl}},\end{aligned} \tag{H6}$$

where the subindex 3 in Φ_3 denotes that this is evaluated for the triple-collision process with conditions (H1) and (H2). The transition probability associated with this process is then given by [see (6.9)]

$$\langle\langle \mathbf{p},\mathbf{p}|\overline{\rho_3}(t)\rangle\rangle \approx -\lambda^4 \frac{v_1^2 v_3^2}{w^2_{\overline{k'}\,\overline{k}}} \int d^2k\; d^2l \int d^2k'\, d^2l'\, \Delta(\mathbf{p},\mathbf{k}',\boldsymbol{l}',\mathbf{k},\boldsymbol{l}) \mathrm{Res}_{\,z=+i\epsilon} \left[\frac{e^{-izt}}{z} \left(\frac{1}{z-w_{pl}} + \frac{1}{z-w_{kp}} \right) \frac{1}{z-w_{kl}} \right] \times \langle\langle \mathbf{k},\boldsymbol{l}|\rho(0)\rangle\rangle. \tag{H7}$$

This has a similar form to (G9). Therefore we have the following.

For $t \ll t_c'$ (during the collision),

$$\langle\langle \mathbf{p},\mathbf{p}|\overline{\rho_3}(t)\rangle\rangle \approx \frac{4\lambda^4 v_1^2 v_3^2}{3 w^2_{\overline{k}\,k'}} 2\pi t\, \delta(\omega_{\overline{k}} - \omega_p). \tag{H8}$$

For $t \gg t_c$ (after the collision),

$$\langle\langle \mathbf{p},\mathbf{p}|\overline{\rho_3}(t)\rangle\rangle \approx \frac{4\lambda^4 v_1^2 v_3^2}{3 w^2_{\overline{k}\,k'}} 2\pi t_c\, \delta(\omega_{\overline{k}} - \omega_p), \tag{H9}$$

where t_c is given in (7.10).

APPENDIX I: RESCATTERING TERM

We shall calculate the rescattering term for the time scales (a) $t \ll t_c'$ and $t \ll t_c$, and (b) $t_c \ll t$ and $t_c' \ll t$, where t_c and t_c' are defined in (7.10). Because at the rescattering point the first collision (between particles 1 and 2) is on-shell, we have that p_{y1} is either k_{y1} or k_{y2}. Hence k_{32} is given by [see (6.25) and (F9)]

$$k_{32}^{\pm} = \frac{2}{\sqrt{3}} \sin(\phi \pm \pi/6) |\overline{\mathbf{k}}|, \tag{I1}$$

where ϕ the incident angle of the incoming particle, with respect to the x_3 axis, and the plus or minus sign corresponds to the cases where the incoming particle is transmitted or reflected by the (12) wall, respectively.

From (7.10) and (I1) we have $t_c < t_c'$. In order to show the transition from the time scales (a) to (b) we shall consider a third time scale (c), $t_c \ll t \ll t_c'$. In this special case the duration of the second collision, t_c', is large because the particle goes nearly parallel to the (23) wall, after colliding with the (12) wall.

(a) For $t \ll t_c'$ and $t \ll t_c$, this time scale is equivalent to

$$\eta |k_{32}^{\pm}| \ll \epsilon, \quad \eta |\overline{\mathbf{k}}| \ll \epsilon, \tag{I2}$$

For this time scale we can approximate the initial condition (4.14) by the plane wave (3.9). This leads to [see (6.9) and (6.6)]

$$\langle\langle \mathbf{p};\mathbf{p}|\overline{\rho(t)}\rangle\rangle \approx \lambda^4 v_1^2 v_3^2 \int d^2k' \int d^2l' \int d^2k \int d^2l\, \Delta(\mathbf{p},\mathbf{k}',\boldsymbol{l}',\mathbf{k},\boldsymbol{l}) \mathrm{Res}_{\,z=+i\epsilon} \left[\frac{1}{z} \left(\frac{1}{z-w_{p\overline{k'}}} + \frac{1}{z-w_{\overline{k'}p}} \right) \frac{1}{z} \left(\frac{1}{z-w_{\overline{k'}\,\overline{k}}} + \frac{1}{z-w_{\overline{k}\,\overline{k'}}} \right) \frac{1}{z} + \frac{1}{z} \left(\frac{1}{z-w_{p\overline{k'}}} \frac{1}{z-w_{p\overline{k}}} \frac{1}{z-w_{\overline{k'}\,\overline{k}}} + \frac{1}{z-w_{\overline{k'}p}} \frac{1}{z-w_{\overline{k}p}} \frac{1}{z-w_{\overline{k}\,\overline{k'}}} \right) \frac{1}{z} \right] \delta(\mathbf{k}-\overline{\mathbf{k}})\, \delta(\boldsymbol{l}-\overline{\mathbf{k}}). \tag{I3}$$

For a large time scale the first term in the brackets makes the dominant contribution, growing as t^2 as the result of the third-order pole at $z = +i\epsilon$, while the second term gives its correction of order t. Performing the integration over intermediate momenta in (I3), for the dominant contribution, we obtain

$$\overline{\rho(\mathbf{p},\mathbf{p},t)} \approx \tfrac{4}{3} \lambda^4 v_1^2 v_3^2 \tfrac{1}{2} (2\pi t)^2\, \delta(w_{p\overline{k'}})\, \delta(w_{p\overline{k}}). \tag{I4}$$

(b) For $t_c \ll t$ and $t_c' \ll t$, we now consider the time scale where all interaction processes are finished. The transition probability approaches a constant in time. As was shown in (G18), this is the situation in which the usual S-matrix theory is applicable.

Substituting (6.24) into (G19), we have

$$\langle\langle \mathbf{p};\mathbf{p}|\overline{\rho(t)}\rangle\rangle = \frac{4\lambda^4 v_1^2 v_3^2}{3} \left(\frac{1}{2\pi} \right)^2 \left| \int_{-\infty}^{+\infty} ds_{y3} \int_{-\infty}^{+\infty} ds_{x3}\, \frac{1}{w_{\overline{k'}p} + 2\eta k_{32} s_{y3} - i\epsilon}\, \frac{1}{w_{\overline{k}p} + 2\eta(\overline{\mathbf{k}}\cdot\mathbf{s}) - i\epsilon}\, e^{-(s_{x3}^2 + s_{y3}^2)/2} \right|^2. \tag{I5}$$

This expression may be rewritten as

$$\langle\langle \mathbf{p};\mathbf{p}|\overline{\rho(t)}\rangle\rangle = \frac{4}{3} \left(\frac{\lambda^2 v_1 v_3}{2\pi} \right)^2 \int d^2s \int d^2u\, \frac{1}{w_{p\overline{k'}} - 2\eta k_{32} s_{y3} + i\epsilon}\, \frac{1}{w_{p\overline{k'}} - 2\eta k_{32} u_{y3} - i\epsilon}\, \frac{1}{w_{p\overline{k}} - 2\eta(\overline{\mathbf{k}}\cdot\mathbf{s}) + i\epsilon}$$

$$\frac{1}{w_{p\overline{k}}-2\eta(\overline{\mathbf{k}}\cdot\mathbf{u})-i\epsilon}\,e^{-(|\mathbf{s}|^2+|\mathbf{u}|^2)/2}. \tag{I6}$$

We are interested in the transition probability taken as a distribution. As shown in (I4), the rescattering term contains two δ functions. Therefore we need two integration variables to make sense of this term. Usually the integration is taken over a set of final momenta (i.e., over the variables p_{xa} and p_{ya}, for $a=1$, 2, or 3). However it is possible to make a change of variables, and integrate over ω_p and $\omega_{\overline{k}'}$ instead. This simplifies the calculations below. We consider the expression

$$I=\int d\omega_p\int d\omega_{\overline{k}'}\langle\langle\mathbf{p};\mathbf{p}|\overline{\rho(t)}\rangle\rangle f(\omega_p,\omega_{\overline{k}'}),$$

where $f(\omega_p,\omega_{\overline{k}'})$ is a test function. The integration region should include the rescattering points, given by $\omega_p=\omega_{\overline{k}'}=\omega_{\overline{k}}$. Then these integrals can be extended from $-\infty$ to $+\infty$, because the contributions from the tail (away from the rescattering peaks) of the transition probability are negligible. The integrals can be performed by contour integration. The result is

$$I^{\pm}\approx(2\pi i)^2\,\frac{4}{3}\left(\frac{\lambda^2 v_1 v_3}{2\pi}\right)^2 f(\omega_{\overline{k}},\omega_{\overline{k}})\int d^2s\int d^2u\,e^{-(|\mathbf{s}|^2+|\mathbf{u}|^2)/2}\,\frac{1}{2\eta k_{32}^{\pm}(u_{y3}-s_{y3})+i\epsilon}\,\frac{1}{2\eta\overline{\mathbf{k}}\cdot(\mathbf{u}-\mathbf{s})+i\epsilon}. \tag{I7}$$

Putting

$$\overline{k_{x3}}=|\overline{\mathbf{k}}|\cos\phi,\quad \overline{k_{y3}}=|\overline{\mathbf{k}}|\sin\phi,$$

we have

$$I^{\pm}=(2\pi i)^2\,\frac{4}{3}\left(\frac{\lambda^2 v_1 v_3}{2\pi}\right)^2 f(\omega_{\overline{k}},\omega_{\overline{k}})\,\frac{1}{2\eta|\overline{\mathbf{k}}|}\,\frac{1}{2\eta k_{32}^{\pm}}\,I_1^{\pm}, \tag{I8}$$

where

$$I_1^{\pm}=\int_{-\infty}^{\infty}ds_{x3}\int_{-\infty}^{\infty}ds_{y3}\int_{-\infty}^{\infty}du_{x3}\int_{-\infty}^{\infty}du_{y3}e^{-(|\mathbf{s}|^2+|\mathbf{u}|^2)/2}\,\frac{1}{(u_{y3}-s_{y3})+i\epsilon\sigma^{\pm}(\phi)}\,\frac{1}{(u_{x3}-s_{x3})\cos\phi+(u_{y3}-s_{y3})\sin\phi+i\epsilon}, \tag{I9}$$

and [see (I1)]

$$\sigma^{\pm}(\phi)=\mathrm{sgn}[\sin(\phi\pm\pi/6)]. \tag{I10}$$

Introducing the variables $v_x\equiv u_{x3}-s_{x3}$ and $v_y\equiv u_{y3}-s_{y3}$, we obtain

$$I_1^{\pm}=\pi\int_{-\infty}^{\infty}dv_x\int_{-\infty}^{\infty}dv_y e^{-(v_x^2+v_y^2)/4}\,\frac{1}{v_y+i\epsilon\sigma^{\pm}(\phi)}\times\frac{1}{v_x\cos\phi+v_y\sin\phi+i\epsilon}. \tag{I11}$$

The integral over v_x can be performed using formula (B1). We then have

$$I_1^{\pm}=\frac{-i\pi^2}{\cos\phi}\int_{-\infty}^{\infty}dv_y e^{-(v_y\sec\phi)^2/4}\,\frac{1}{v_y+i\epsilon\sigma^{\pm}(\phi)}\times\left[\mathrm{sgn}(\cos\phi)+\frac{2i}{\sqrt{\pi}}\,\mathrm{erfi}\left(\frac{v_y\tan\phi}{2}\right)\right]. \tag{I12}$$

The first term can be evaluated using (B10), to obtain

$$-\frac{\pi^3}{|\cos\phi|}\,\sigma^{\pm}(\phi). \tag{I13}$$

The second term can be written as

$$I_2=\frac{2\pi^{3/2}}{|\cos\phi|}\,I_3, \tag{I14}$$

where (with $y\equiv v_y|\sec\phi|/2$)

$$I_3=\int_{-\infty}^{\infty}dy\;e^{-y^2}\,\frac{1}{y}\,\mathrm{erfi}(y\,\sin\phi). \tag{I15}$$

Taking the derivative of I_3 with respect to $\sin\phi$, and changing the integration variable to $x\equiv y\sin\phi$, we obtain

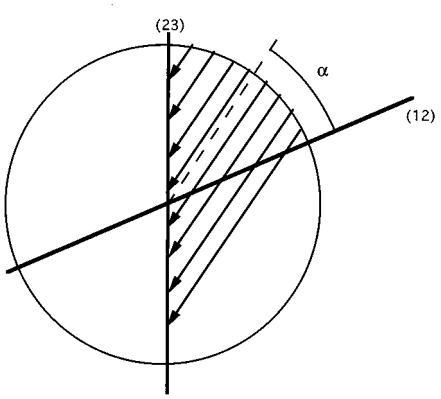

FIG. 16. In this rescattering process the (12) wall transmits incoming beams (represented by the arrows), which then collide with the (23) wall. The wave packet is represented by the circle. Only region α of the wave packet can go through this collision sequence.

$$\frac{dI_3}{d(\sin\phi)}=\int_{-\infty}^{\infty}dy\ e^{-y^2}\mathrm{erfi}'(y\ \sin\phi)$$

$$=\frac{1}{|\sin\phi|}\int_{-\infty}^{\infty}dx\ e^{-x^2/\sin^2\phi}\mathrm{erfi}'(x).$$

As $\mathrm{erfi}'(x)=e^{x^2}$, we have

$$\frac{dI_3}{d(\sin\phi)}=\frac{\sqrt{\pi}}{|\cos\phi|},$$

which leads to

$$I_3=\sqrt{\pi}\int_0^{\phi}d\phi'\ \mathrm{sgn}(\cos\phi'). \tag{I16}$$

Hence

$$I_1^{\pm}=\frac{-\pi^3}{|\cos\phi|}\left[\sigma^{\pm}(\phi)-\frac{2}{\pi}\,\xi(\phi)\right], \tag{I17}$$

where

$$\begin{aligned}\xi(\phi)&=\phi \quad \text{for}\ -\pi/2<\phi<\pi/2,\\ \pi-\phi&\quad \text{for}\ \pi/2<\phi<\pi,\\ -\pi-\phi&\quad \text{for}\ -\pi<\phi<-\pi/2.\end{aligned} \tag{I18}$$

With $t_c=\sqrt{\pi}/(4\eta|\overline{\mathbf{k}}|)$ and $t_c'^{\pm}=\sqrt{\pi}/(4\eta|k_{32}^{\pm}|)$ we have, from (I8),

$$I^{\pm}=\tfrac{4}{3}\lambda^4 v_1^2 v_3^2 f(\omega_{\overline{k}},\omega_{\overline{k}})\,\frac{2\pi t_c}{|\cos\phi|}\,2\pi t_c'^{\pm}F^{\pm}(\phi), \tag{I19}$$

where

$$F^{\pm}(\phi)=1-\frac{2}{\pi}\,\sigma^{\pm}(\phi)\xi(\phi). \tag{I20}$$

Hence we have

$$\langle\langle\mathbf{p};\mathbf{p}|\overline{\rho(t)}\rangle\rangle^{\pm}\approx\tfrac{4}{3}\lambda^4 v_1^2 v_3^2 2\pi\delta(w_{p\overline{k}'})2\pi\delta(w_{p\overline{k}})\,\frac{t_c}{|\cos\phi|}$$

$$\times t_c'^{\pm}F^{\pm}(\phi). \tag{I21}$$

$t_c/|\cos\phi|$ is the duration of the first collision [the cosine gives the component of the momentum of the wave packet perpendicular to the (12) wall], while t_c' is the duration of the second collision. The factor $F^{\pm}(\phi)$ accounts for the fact that, depending on the incident angle ϕ, a fraction of the wave packet will not collide with the (23) wall after colliding with the (12) wall. In Fig. 16 we show how only a fraction α of the wave packet (indicated by a circle) can have a (12) collision followed by a (23) collision. We are taking the plus branch of (I21); that is, the transmitted beams originated by the (12) collision.

(c) For $t_c\ll t\ll t_c'$, the time scale is equivalent to

$$\eta|k_{32}^{\pm}|\ll\epsilon\ll\eta|\overline{\mathbf{k}}|, \tag{I22}$$

where both η and ϵ are small quantities. The conditions for the shape of the initial wave packet (4.15), as well as (6.23), lead to [see (6.24) and (6.26)]

$$O(|w_{kl}|)=\eta|\overline{\mathbf{k}}|,\quad O(|w_{k'l'}|)=\eta|k_{32}|. \tag{I23}$$

Let us first consider the contribution for the first term inside the brackets (6.6) that corresponds to diagrams (a)–(d) in Fig. 12. We can rewrite this as

$$\Phi_{ad}(\mathbf{p},\mathbf{k}',\boldsymbol{l}',\mathbf{k},\boldsymbol{l},z)=\lambda^4 v_1^2 v_3^2\Delta(\mathbf{p},\mathbf{k}',\boldsymbol{l}',\mathbf{k},\boldsymbol{l})\,\frac{1}{z}\,\frac{1}{z-w_{pl'}}\,\frac{1}{z-w_{k'p}}\left(1+\frac{z}{z-w_{k'l'}}\right)\frac{1}{z-w_{k'l}}\,\frac{1}{z-w_{kl'}}\left(1+\frac{z-w_{k'l'}}{z-w_{kl}}\right). \tag{I24}$$

With conditions (I22) and (I23) the above expression is (for $|z|\sim\epsilon$)

$$\Phi_{ad}(\mathbf{p},\mathbf{k}',\mathbf{l}',\mathbf{k},\mathbf{l},z)\approx 2\lambda^4 v_1^2 v_3^2 \Delta(\mathbf{p},\mathbf{k}',\mathbf{l}',\mathbf{k},\mathbf{l})\,\frac{1}{z}\,\frac{1}{z-w_{p\overline{k'}}}\,\frac{1}{z-w_{\overline{k'}p}}\,\frac{1}{z-w_{k'l}}\,\frac{1}{z-w_{kl'}}$$

$$\approx \lambda^4 v_1^2 v_3^2 \Delta(\mathbf{p},\mathbf{k}',\mathbf{l}',\mathbf{k},\mathbf{l})\,\frac{1}{z^2}\left[\frac{1}{z-w_{p\overline{k'}}}+\frac{1}{z-w_{\overline{k'}p}}\right]\left[\frac{1}{z-w_{\overline{k'}\overline{k}}+2\,\eta\overline{\mathbf{k}}\cdot\mathbf{u}}\,\frac{1}{-z-w_{\overline{k'}\overline{k}}+2\,\eta\overline{\mathbf{k}}\cdot\mathbf{s}}\right]. \quad \text{(I25)}$$

Because of the second-order pole at $z=+i\epsilon$, its residue makes the linearly growing contribution of t for the transition probability (G16) for large time scales.

With conditions (I22) and (I23), the reader can easily verify by a similar manipulation that the second term inside the brackets in (6.6) [corresponding to diagrams (e) and (f) in Fig. 12] has only a simple pole at $z=+i\epsilon$. Hence this contribution does not grow in time, and is negligible for large time scales.

The first term inside the brackets in (I25) gives a factor $-2\pi t\,\delta(w_{p\overline{k'}})$ [see (G16) and (G17)]. On the other hand, the integrations over **s** and **u** of the second term inside brackets can be written, for $z=i\epsilon$, as

$$\left|\int d^2\mathbf{s}\,\frac{1}{-i\epsilon-w_{\overline{k'}\overline{k}}+2\,\eta\overline{\mathbf{k}}\cdot\mathbf{s}}\,\frac{1}{2\pi}\,e^{-|\mathbf{s}|^2/2}\right|^2. \quad \text{(I26)}$$

The integration has a structure similar to the integration in (G12). Hence, by a similar evaluation, (I26) gives a factor $-2\pi t_c\,\delta(w_{\overline{k\,k'}})$. Finally, the integrations over $\mathbf{k}'$ and $\mathbf{l}'$ give a $\frac{4}{3}$ factor [see (7.13)]. Hence we have

$$\overline{\rho_4}(\mathbf{p},\mathbf{p},t)\approx\tfrac{4}{3}\lambda^4 v_1^2 v_3^2 2\pi t\,\delta(w_{p\overline{k'}})2\pi t_c\,\delta(w_{\overline{k\,k'}}), \quad \text{(I27)}$$

where the suffix 4 in $\overline{\rho_4}$ denotes that this is evaluated for (I22) with the condition (I23). Therefore, the dominant contribution of the transition probability comes from the rescattering process (i.e., the on-on shell process) and it grows linearly in time in the intermediate time scale $t_c \ll t \ll t_c'$.

APPENDIX J: PROOF OF (9.5)

By a straightforward calculation, one can verify the relation (for any real ϵ)

$$\left[\frac{1}{(w+i\epsilon)^2}-\text{c.c.}\right](e^{iwt}-e^{-iwt})+\left[\frac{1}{(w-i\epsilon)^2}\,(1-e^{-iwt})+\text{c.c.}\right]+\frac{1}{2}\left|\left(\frac{1}{w-i\epsilon}-\text{c.c.}\right)(1-e^{iwt})\right|^2=\left|\frac{1-e^{iwt}}{w+i\epsilon}\right|^2. \quad \text{(J1)}$$

In the limit $\epsilon\to 0+$, the last term on the left-hand side vanishes in the sense of distributions with suitable test functions. Moreover, we have (for $\epsilon\to 0+$)

$$2\pi i\,\delta'(w)=\frac{1}{(w+i\epsilon)^2}-\text{c.c.} \quad \text{(J2)}$$

and

$$4\left[\frac{\sin(wt/2)}{w}\right]^2=\left|\frac{1-e^{iwt}}{w+i\epsilon}\right|^2. \quad \text{(J3)}$$

Under the integration over w, we perform the integration by parts for $\delta'(w)$. Then we have (for $\epsilon\to 0+$)

$$4\left[\frac{\sin(wt/2)}{w}\right]^2=\pi i\,\delta'(w)(e^{iwt}-e^{-iwt})+\left[\frac{1}{(w-i\epsilon)^2}\,(1-e^{iwt})+\text{c.c.}\right]=2\pi\delta(w)t+\left[\frac{1}{(w-i\epsilon)^2}\,(1-e^{iwt})+\text{c.c.}\right], \quad \text{(J4)}$$

which is the desired result (9.5).

[1] *Quantum Scattering Theory. Selected Papers*, edited by M. Ross (Indiana University Press, Bloomington, 1963).
[2] C. C. Grosjean, *Formal Theory of Scattering Phenomena* (Institut Interuniversitaire des Sciences Nucleaires, Bruxelles, 1960).
[3] M. L. Goldberger and K. M. Watson, *Collision Theory* (Wiley, New York, 1965).
[4] R. G. Newton, *Scattering Theory of Waves and Particles* (McGraw-Hill, New York, 1966).
[5] R. G. Newton, Ann. Phys. **74**, 324 (1972).
[6] R. G. Newton, Phys. Rev. A **14**, 642 (1976).
[7] P. Resibois, Physica **27**, 33 (1961).
[8] P. Resibois, Physica **31**, 645 (1965).
[9] T. Petrosky and I. Prigogine, Chaos Solitons Fractals **4**, 311 (1994).
[10] T. Petrosky and I. Prigogine, Chaos Solitons Fractals (to be published).
[11] T. Petrosky and G. Ordonez (unpublished).
[12] I. Prigogine, *NonEquilibrium Statistical Mechanics* (Wiley Interscience, New York, 1962).
[13] C. N. Yang, Phys. Rev. Lett. **19**, 1312 (1967).
[14] H. B. Thacker, Phys. Rev. D **14**, 3508 (1976).

[15] E. H. Lieb and W. Liniger, Phys. Rev. **130**, 1605 (1963).
[16] T. Petrosky, I. Prigogine, and G. Ordonez (unpublished).
[17] J. B. MacGuire, J. Math. Phys. **5**, 622 (1964).
[18] L. D. Faddeev and S. P Merkuriev, *Quantum Scattering Theory for Several Particle Systems* (Kluwer Academic, Dordrecht, 1993).
[19] M. Rubin, R. Sugar, and G. Tiktopoulos, Phys. Rev. **146**, 1130 (1966).
[20] T. Petrosky and I. Prigogine, Physica A **175**, 146 (1991).
[21] T. Petrosky and I. Prigogine, Adv. Chem. Phys. (to be published).
[22] I. S. Gradshteyn and I. M. Ryzhik, *Table of Integrals, Series, and Products* (Academic, New York, 1980).